Measurement of the Deuteron Structure Function F_2 in the Resonance Region and Evaluation of Its Moments

M. Osipenko,[1,2] G. Ricco,[1] S. Simula,[3] M. Battaglieri,[1] M. Ripani,[1] G. Adams,[31] P. Ambrozewicz,[13] M. Anghinolfi,[1] B. Asavapibhop,[25] G. Asryan,[40] G. Audit,[8] H. Avakian,[18,35] H. Bagdasaryan,[29] N. Baillie,[39] J.P. Ball,[4] N.A. Baltzell,[34] S. Barrow,[14] V. Batourine,[23] K. Beard,[22] I. Bedlinskiy,[21] M. Bektasoglu,[28,*] M. Bellis,[31,6] N. Benmouna,[15] A.S. Biselli,[31,6] B.E. Bonner,[32] S. Bouchigny,[35,19] S. Boiarinov,[21,35] R. Bradford,[6] D. Branford,[11] W.K. Brooks,[35] S. Bültmann,[29] V.D. Burkert,[35] C. Butuceanu,[39] J.R. Calarco,[26] S.L. Careccia,[29] D.S. Carman,[28] A. Cazes,[34] S. Chen,[14] P.L. Cole,[35,17] A. Coleman,[39,†] P. Coltharp,[14] D. Cords,[35,‡] P. Corvisiero,[1] D. Crabb,[38] J.P. Cummings,[31] E. De Sanctis,[18] R. DeVita,[1] P.V. Degtyarenko,[35] H. Denizli,[30] L. Dennis,[14] A. Deur,[35] K.V. Dharmawardane,[29] C. Djalali,[34] G.E. Dodge,[29] J. Donnelly,[16] D. Doughty,[9,35] P. Dragovitsch,[14] M. Dugger,[4] S. Dytman,[30] O.P. Dzyubak,[34] H. Egiyan,[39,35,§] K.S. Egiyan,[40] L. Elouadrhiri,[9,35] A. Empl,[31] P. Eugenio,[14] R. Fatemi,[38] G. Fedotov,[2] R.J. Feuerbach,[6,35] T.A. Forest,[29] H. Funsten,[39] M. Garçon,[8] G. Gavalian,[29] G.P. Gilfoyle,[33] K.L. Giovanetti,[22] F.X. Girod,[8] J.T. Goetz,[5] E. Golovatch,[1,¶] C.I.O. Gordon,[16] R.W. Gothe,[34] K.A. Griffioen,[39] M. Guidal,[19] M. Guillo,[34] N. Guler,[29] L. Guo,[35] V. Gyurjyan,[35] C. Hadjidakis,[19] R.S. Hakobyan,[7] J. Hardie,[9,35] D. Heddle,[9,35] F.W. Hersman,[26] K. Hicks,[28] I. Hleiqawi,[28] M. Holtrop,[26] J. Hu,[31] M. Huertas,[34] C.E. Hyde-Wright,[29] Y. Ilieva,[15] D.G. Ireland,[16] B.S. Ishkhanov,[2] M.M. Ito,[35] D. Jenkins,[37] H.S. Jo,[19] K. Joo,[38,35,10] H.G. Juengst,[29] J.D. Kellie,[16] M. Khandaker,[27] K.Y. Kim,[30] K. Kim,[23] W. Kim,[23] A. Klein,[29] F.J. Klein,[35,13,7] A.V. Klimenko,[29] M. Klusman,[31] M. Kossov,[21] L.H. Kramer,[13,35] V. Kubarovsky,[31] J. Kuhn,[31,6] S.E. Kuhn,[29] J. Lachniet,[6] J.M. Laget,[8] J. Langheinrich,[34] D. Lawrence,[25] T. Lee,[26] Ji Li,[31] A.C.S. Lima,[15] K. Livingston,[16] K. Lukashin,[35,7] J.J. Manak,[35] C. Marchand,[8] S. McAleer,[14] B. McKinnon,[16] J.W.C. McNabb,[6] B.A. Mecking,[35] S. Mehrabyan,[30] J.J. Melone,[16] M.D. Mestayer,[35] C.A. Meyer,[6] K. Mikhailov,[21] R. Minehart,[38] M. Mirazita,[18] R. Miskimen,[25] V. Mokeev,[35,2] L. Morand,[8] S.A. Morrow,[19,8] J. Mueller,[30] G.S. Mutchler,[32] P. Nadel-Turonski,[15] J. Napolitano,[31] R. Nasseripour,[13,**] S. Niccolai,[15,19] G. Niculescu,[28,22] I. Niculescu,[15,35,22] B.B. Niczyporuk,[35] R.A. Niyazov,[35] M. Nozar,[35] G.V. O'Rielly,[15] A.I. Ostrovidov,[14] K. Park,[23] E. Pasyuk,[4] S.A. Philips,[15] J. Pierce,[38] N. Pivnyuk,[21] D. Pocanic,[38] O. Pogorelko,[21] E. Polli,[18] S. Pozdniakov,[21] B.M. Preedom,[34] J.W. Price,[5] Y. Prok,[38,35,††] D. Protopopescu,[26,16] L.M. Qin,[29] B.A. Raue,[13,35] G. Riccardi,[14] B.G. Ritchie,[4] F. Ronchetti,[18] G. Rosner,[16] P. Rossi,[18] D. Rowntree,[24] P.D. Rubin,[33] F. Sabatié,[8] C. Salgado,[27] J.P. Santoro,[37,35] V. Sapunenko,[1,35] R.A. Schumacher,[6] V.S. Serov,[21] Y.G. Sharabian,[35] J. Shaw,[25] A.V. Skabelin,[24] E.S. Smith,[35] L.C. Smith,[38] D.I. Sober,[7] A. Stavinsky,[21] S.S. Stepanyan,[23] S. Stepanyan,[35,40] B.E. Stokes,[14] P. Stoler,[31] S. Strauch,[15] R. Suleiman,[24] M. Taiuti,[1] S. Taylor,[32] D.J. Tedeschi,[34] U. Thoma,[35,20,12,‡‡] R. Thompson,[30] A. Tkabladze,[28] L. Todor,[6] C. Tur,[34] M. Ungaro,[31,10] M.F. Vineyard,[36,33] A.V. Vlassov,[21] L.B. Weinstein,[29] D.P. Weygand,[35] M. Williams,[6] E. Wolin,[35] M.H. Wood,[34,§§] A. Yegneswaran,[35] J. Yun,[29] L. Zana,[26] and J. Zhang[29]

(The CLAS Collaboration)

[1]*INFN, Sezione di Genova, 16146 Genova, Italy*
[2]*Moscow State University, General Nuclear Physics Institute, 119899 Moscow, Russia*
[3]*Università di ROMA III, 00146 Roma, Italy*
[4]*Arizona State University, Tempe, Arizona 85287-1504*
[5]*University of California at Los Angeles, Los Angeles, California 90095-1547*
[6]*Carnegie Mellon University, Pittsburgh, Pennsylvania 15213*
[7]*Catholic University of America, Washington, D.C. 20064*
[8]*CEA-Saclay, Service de Physique Nucléaire, F91191 Gif-sur-Yvette,Cedex, France*
[9]*Christopher Newport University, Newport News, Virginia 23606*
[10]*University of Connecticut, Storrs, Connecticut 06269*
[11]*Edinburgh University, Edinburgh EH9 3JZ, United Kingdom*
[12]*Emmy-Noether Foundation, Germany*
[13]*Florida International University, Miami, Florida 33199*
[14]*Florida State University, Tallahassee, Florida 32306*
[15]*The George Washington University, Washington, DC 20052*
[16]*University of Glasgow, Glasgow G12 8QQ, United Kingdom*
[17]*Idaho State University, Pocatello, Idaho 83209*
[18]*INFN, Laboratori Nazionali di Frascati, Frascati, Italy*
[19]*Institut de Physique Nucleaire ORSAY, Orsay, France*
[20]*Institute für Strahlen und Kernphysik, Universität Bonn, Germany*
[21]*Institute of Theoretical and Experimental Physics, Moscow, 117259, Russia*
[22]*James Madison University, Harrisonburg, Virginia 22807*

[23]Kyungpook National University, Daegu 702-701, South Korea
[24]Massachusetts Institute of Technology, Cambridge, Massachusetts 02139-4307
[25]University of Massachusetts, Amherst, Massachusetts 01003
[26]University of New Hampshire, Durham, New Hampshire 03824-3568
[27]Norfolk State University, Norfolk, Virginia 23504
[28]Ohio University, Athens, Ohio 45701
[29]Old Dominion University, Norfolk, Virginia 23529
[30]University of Pittsburgh, Pittsburgh, Pennsylvania 15260
[31]Rensselaer Polytechnic Institute, Troy, New York 12180-3590
[32]Rice University, Houston, Texas 77005-1892
[33]University of Richmond, Richmond, Virginia 23173
[34]University of South Carolina, Columbia, South Carolina 29208
[35]Thomas Jefferson National Accelerator Facility, Newport News, Virginia 23606
[36]Union College, Schenectady, NY 12308
[37]Virginia Polytechnic Institute and State University, Blacksburg, Virginia 24061-0435
[38]University of Virginia, Charlottesville, Virginia 22901
[39]College of William and Mary, Williamsburg, Virginia 23187-8795
[40]Yerevan Physics Institute, 375036 Yerevan, Armenia
(Dated: October 21, 2005)

Inclusive electron scattering off the deuteron has been measured to extract the deuteron structure function F_2 with the CEBAF Large Acceptance Spectrometer (CLAS) at the Thomas Jefferson National Accelerator Facility. The measurement covers the entire resonance region from the quasi-elastic peak up to the invariant mass of the final-state hadronic system $W \approx 2.7$ GeV with four-momentum transfers Q^2 from 0.4 to 6 (GeV/c)^2. These data are complementary to previous measurements of the proton structure function F_2 and cover a similar two-dimensional region of Q^2 and Bjorken variable x. Determination of the deuteron F_2 over a large x interval including the quasi-elastic peak as a function of Q^2, together with the other world data, permit a direct evaluation of the structure function moments for the first time. By fitting the Q^2 evolution of these moments with an OPE-based twist expansion we have obtained a separation of the leading twist and higher twist terms. The observed Q^2 behaviour of the higher twist contribution suggests a partial cancellation of different higher twists entering into the expansion with opposite signs. This cancellation, found also in the proton moments, is a manifestation of the "duality" phenomenon in the F_2 structure function.

PACS numbers: 12.38.Cy, 12.38.Lg, 12.38.Qk, 13.60.Hb
Keywords: moments, deuteron, nucleon structure, higher twists, QCD, OPE

I. INTRODUCTION

Inclusive lepton scattering off the deuteron has provided a wealth of information about internal nucleon structure and nuclear phenomena. Since a free neutron target does not exist, the deuteron is the simplest target for the study of neutron structure functions. The weak coupling between the two nucleons in the deuteron, corresponding to a large space-time separation, suggests that the nucleus can be described as a non-relativistic proton and neutron moving inside some mean potential. To this end, the momentum distribution of the deuteron was established with high precision from the quasi-elastic and NN reactions, and approaches describing the Fermi motion of the nucleons were developed. This naive picture, however, was superseded by experiments when the European Muon Collaboration (EMC) discovered deviations of the measured nuclear structure function F_2 from that of a free proton and neutron convoluted with Fermi smearing (a phenomenon known as the EMC-effect [1]). Different attempts to explain the EMC-effect have been undertaken, but without reaching a unified and, therefore, definitive description.

A Quantum Chromodynamics (QCD)-based approach, on the other hand, can handle the nuclear structure functions in a model-independent manner. This method is based on the Operator Product Expansion (OPE) of the structure function moments, whose Q^2-evolution is known in QCD at leading twist and some fixed order in α_S. However, the leading twist picture is valid only in

*Current address:Sakarya University, Sakarya, Turkey
†Current address:Systems Planning and Analysis, Alexandria, Virginia 22311
‡Deceased
§Current address:University of New Hampshire, Durham, New Hampshire 03824-3568
¶Current address:Moscow State University, General Nuclear Physics Institute, 119899 Moscow, Russia
**Current address:University of South Carolina, Columbia, South Carolina 29208
††Current address:Massachusetts Institute of Technology, Cambridge, Massachusetts 02139-4307
‡‡Current address:Physikalisches Institut der Universitaet Giessen, 35392 Giessen, Germany
§§Current address:University of Massachusetts, Amherst, Massachusetts 01003

Deep Inelastic Scattering (DIS) and for not very large x values. Beyond these kinematic boundaries, e.g. in the region of large x and moderate Q^2, new poorly established physics appears. This kinematic domain has a particular interest because multi-parton correlation phenomena manifest themselves as deviations from perturbative QCD (pQCD) predictions.

In the one photon exchange approximation, the cross section for inclusive electron scattering off a nucleus is described by the total absorption of the virtual photon by the nucleus. The optical theorem relates the total virtual photoabsorption cross section to the forward Compton scattering amplitude of the virtual photon on the nucleus. The latter amplitude, in general, can be represented as a product of two hadronic currents separated by a certain space-time interval ζ^2. In the Bjorken limit, the interval $\zeta^2 \to 0$ (while the light-cone ζ^- component is fixed) allows one to apply the OPE to the product of non-local hadronic currents. This leads to a relation where the moments M_n^{CN} (Cornwall-Norton definition [2]) of the nucleon (nucleus with mass A) structure functions, defined as:

$$M_n^{CN}(Q^2) = \int_0^A dx x^{(n-2)} F_2(x, Q^2), \quad n \geq 2, n \text{ even}, \tag{1}$$

are expanded as a series of inverse powers (twists) of the four-momentum transfer Q^2 (for details see Ref. [3]). A study of the Q^2 dependence of these moments, therefore, would permit one to isolate different terms of this series, each representing distinct physical processes in QCD. The first term in the expansion represents the leading twist, i.e. the limit of asymptotic freedom, while higher terms account for the interactions among partons inside the nucleon. The contribution of these multi-parton correlations to the nucleon wave function increases in the region of large x (corresponding to high moment order n) and low Q^2.

For the proton, a careful study of the multi-parton correlation contribution, which included a global analysis of all the world's data on the proton structure function F_2, has been recently described in Ref. [4]. This analysis could not be done for the deuteron structure function because of the lack of data in the region of the quasi-elastic peak, and because of the scarcity of data in the resonance region. However, a previous analysis from Ref. [5], based on fits of the structure function F_2, showed a modification of the scaling behaviour of the nucleon structure function F_2 in the nuclear medium. The Hall C Collaboration at Jefferson Lab has recently provided high quality data in this kinematic region [6], but the exclusion of the quasi-elastic peak in this measurement prevented further studies of these data in terms of QCD.

In this paper we report on a measurement of unpolarized inclusive electron scattering from deuterium taken with the CLAS detector in Hall B at Jefferson Lab. The data span a wide continuous two-dimensional region in x and Q^2 (see Fig. 1). The F_2 structure function of the deuteron was extracted over the entire resonance region

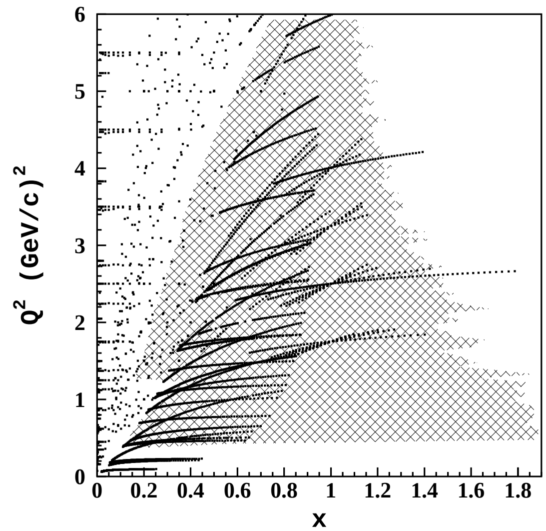

FIG. 1: Experimental data on the deuteron structure function $F_2(x, Q^2)$ used for the moment evaluation in the CLAS kinematic region. The points show world data from Refs. [6, 7, 8, 9, 10, 11, 12, 13, 14, 15, 16, 17, 18, 19, 20]. The shaded area shows CLAS data.

($W \leq 2.7$ GeV) below $Q^2 = 6$ (GeV/c)^2. This measurement, together with existing world data, allowed for the first time the evaluation of the first four F_2 moments of the deuteron down to $Q^2 \sim 0.4$ (GeV/c)^2.

In section II we review the F_2 moments in the framework of pQCD. In section III we discuss improvements in the data analysis implemented since the first unpolarized inclusive measurement at CLAS, along with some details of the evaluation of the moments. For other details of the analysis we refer to Ref. [4]. Finally, in Section IV we discuss the interpretation of the results.

II. MOMENTS OF THE STRUCTURE FUNCTION F_2

Measured structure functions for a free nucleon target in the DIS regime are related to parton momentum distributions of the nucleon. For a nuclear target this relation is not direct since it is necessary to account for effects of the Fermi motion, meson exchange currents, off-shellness of the nucleon and final state interactions (FSI). Nevertheless, the OPE of the structure function moments of the nuclear structure function is still applicable in the same way as for the free nucleon. The n-th Cornwall-Norton moment [2] of the (asymptotic) structure function $F_2(x, Q^2)$ for a massless target can be expanded as:

$$M_n^{CN}(Q^2) = \sum_{\tau=2k}^{\infty} E_{n\tau}(\mu_r, \mu_f, Q^2) O_{n\tau}(\mu_f) \left(\frac{\mu^2}{Q^2}\right)^{\frac{1}{2}(\tau-2)}, \tag{2}$$

where $k = 1, 2, ..., \infty$, μ_f (μ_r) is the factorization (renormalization) scale[1], μ is an arbitrary reference scale, $O_{n\tau}(\mu_r)$ is the reduced matrix element of the local operators with definite spin n and twist τ (dimension minus spin) which is related to the non-perturbative structure of the target. $E_{n\tau}(\mu_r, \mu_f, Q^2)$ is a dimensionless coefficient function describing the small distance behaviour, which can be perturbatively expressed as a power expansion of the running coupling constant $\alpha_s(Q^2)$. Moreover, the leading twist ($\tau = 2$) Q^2 dependence remains unchanged with respect to the free nucleon target and all the nuclear effects appear either in the higher twist terms ($\tau > 2$) or in the reduced matrix element $O_{n2}(\mu_r)$, which does not depend on Q^2. The non-zero mass of the target[2] leads to additional M^2/Q^2 power corrections (kinematic twists) which mix operators of different spin. These target mass corrections can be accounted for by use of Nachtmann [22] moments $M_n^N(Q^2)$ instead of the usual (massless) Cornwall-Norton moments. In the asymptotic DIS limit M^2/Q^2 terms become negligible and both definitions coincide. The Nachtmann moments for the deuteron structure function are defined as follows:

$$M_n^N(Q^2) = \int_0^2 dx \frac{\xi^{n+1}}{x^3} F_2(x, Q^2) \left[\frac{3 + 3(n+1)r + n(n+2)r^2}{(n+2)(n+3)} \right], \quad (3)$$

where $r = \sqrt{1 + 4M^2x^2/Q^2}$, M is the proton mass and $\xi = 2x/(1 + r)$.

The evolution of the leading twist term is known for the first four moments up to Next-to-Next-to-Leading Order (NNLO). However, if one wants to extend the analysis down to $Q^2 \approx M^2$ and to large x, where the rest of the perturbative series becomes significant, one needs to account for additional logarithmic corrections due to soft gluon radiation [21, 23]. These corrections re-summed in the moment space to all orders of α_S appear due to an imbalance of the virtual and real gluon emission at $x \to 1$. Since the Q^2-evolution of the higher twist terms, related to quark-quark and quark-gluon correlations, is unknown, their logarithmic QCD behaviour is parameterized and the corresponding anomalous dimensions are extracted from the data.

Measurement of the Nachtmann moments $M_n^N(Q^2)$ in the intermediate Q^2 range ($0.5 < Q^2 < 10$ (GeV/c)^2) allows a model-independent separation of the total higher twist contribution from the leading twist. Comparison of the higher twist contribution in the deuteron to that in the free proton provides important insight into the nucleon structure modifications inside nuclear matter.

[1] We are working in the Soft Gluon Re-summation (SGR) scheme[21], where $\mu_f^2 = \mu_r^2 = Q^2$.

[2] In the leading twist approximation the target is a nucleon inside the deuteron.

III. DATA ANALYSIS

The data were collected at Jefferson Lab in Hall B with the CLAS using a liquid-deuterium target with thickness 0.81 g/cm^2 during the electron beam running periods in March-April 2000 and January-March 2002. The average beam-target luminosity for these periods was 6×10^{33} cm^{-2}s^{-1}. To maximize the interval in Q^2 and x, data were taken at two different electron beam energies: $E_0 = 2.474$ and 5.770 GeV. The accumulated statistics at the two energies is large enough ($> 10^9$ triggers) to allow for the extraction of the inclusive cross section with a small statistical uncertainty ($\leq 5\%$) in small x and Q^2 bins (Δx =0.009, ΔQ^2 =0.05 (GeV/c)^2).

The CLAS is a magnetic spectrometer [24] based on a six-coil torus magnet whose field is primarily oriented along the azimuthal direction. The sectors, located between the magnet coils, are individually instrumented to form six independent magnetic spectrometers. The particle detection system includes drift chambers (DC) for track reconstruction [25], scintillation counters (SC) for time of flight measurements [26], Cherenkov counters (CC) for electron identification [27], and electromagnetic calorimeters (EC) to measure neutrals and to improve electron-pion separation [28]. The EC detectors, which have a granularity defined by triangular cells in a plane perpendicular to the incoming particles, are used to study the shape of the electromagnetic shower and are longitudinally divided into two parts with the inner part acting as a pre-shower. Charged particles can be detected and identified for momenta down to 0.2 (GeV/c) and for polar angles between 8° and 142°. The CLAS superconducting coils limit the acceptance for charged hadrons from about 80% at $\theta = 90°$ to about 50% at forward angles ($\theta = 20°$). The total angular acceptance for electrons is about 1.5 sr. Electron momentum resolution is a function of the scattered electron angle and varies from 0.5% for $\theta \leq 30°$ up to 1-2% for $\theta > 30°$. The angular resolution is approximately constant, approaching 1 mrad for polar and 4 mrad for azimuthal angles: the resolution for the momentum transfer ranges therefore from 0.2 up to 0.5 %. The scattered electron missing mass (W) resolution was estimated to be 2.5 MeV for a beam energy less than 3 GeV and about 7 MeV for larger energies. To study all possible multi-particle states, the acquisition trigger was configured to require at least one electron candidate in any of the sectors, where an electron candidate was defined as the coincidence of a signal in the EC and Cherenkov modules for any one of the sectors.

The data analysis procedure has been described in detail in Refs. [4, 29]. Therefore, in this article we focus on changes and improvements in the analysis. The most important improvements, leading to a significant reduction of the estimated systematic uncertainties relative to those of Ref. [4], are described in the following sections.

A. Electron Identification

The pion contamination observed in Ref. [4] in the electron candidate sample was found to be due to random coincidences between a pion track measured in the DC and a noise pulse in a CC photomultiplier tube (PMT) (typically corresponding to one photo-electron). These coincidences can be greatly reduced by means of better matching between the CC hits and the measured tracks.

Each CLAS sector consists of 18 CC segments, each containing two PMTs. Therefore, the probability of a coincidence is the product of probabilities to have a noise signal in one of 36 PMTs together with a negative pion track in a time interval, Δt =150 ns, which corresponds to the trigger window time. The average CC PMT noise rate R^{PMT} in CLAS was measured to be ≈42 kHz. For our typical running conditions, the average rate of negatively charged hadrons within our geometrical EC fiducial cuts (used to ensure the shower is fully contained with the detector) that have an appropriate EC signal is of the order of R^{h-} ≈2.3 kHz. This gives an estimate of the possible contamination:

$$R^{1phe} = R^{PMT} R^{h-} \Delta t \approx 15 \text{ Hz} \quad , \tag{4}$$

which should be compared to the electron rate R^{e-} ≈250 Hz, using the same cuts. Therefore, the expected contamination is of the order of 6% overall. In contrast, for small momenta $p < 1$ (GeV/c) and large scattering angles, $\theta > 30°$, R^{h-} ≈1.7 kHz and R^{e-} ≈100 Hz, resulting in a contamination of 12%.

In order to reduce the contamination of the coincidences between a hadron track and a CC noise signal, we applied geometrical and time matching requirements between the CC signal and the measured track in the following way:

1. we defined a CC projective plane, an imaginary plane behind the CC detector where Cherenkov radiation would arrive if it were to propagate the same distance from the emission point to the PMT without any reflections in the mirror system;

2. for each CC segment we found the polar angle from the CLAS center to the image of the CC segment center and to the images of the CC edges;

3. the impact point and the direction of the track in the SC plane, as measured in the DC, were used to obtain the measured polar angle θ in the projective plane for each electron candidate event. We fitted the θ distributions separately for each CC segment in order to extract their measured width σ_p;

4. for each CC segment we applied a cut:

$$|\theta_{track} - \theta_{hit}| < 3\sigma_p \tag{5}$$

which was intended to remove those electron event candidates for which the track impact point in the CC was far away from the segment where the hit was detected. In Fig. 2 an example of the θ distribution is shown for one segment and the cut applied is indicated by dashed lines. To clearly identify the contribution of the coincidences and check the efficiency of the cut we separated events outside the single photo-electron peak (which contains most of the pion contamination) by applying a cut, $N_{phe} > 2.5$. These electron candidate events with reduced pion contamination are shown in Fig. 2 by the hatched histogram. The difference between the empty and the hatched histogram in the figure is therefore mostly due to the pion contamination;

5. to perform time matching between the CC and SC hits of the electron candidate event we studied the distribution of the time-offset of the CC signal with respect to the SC. For each CC segment we measured Δt^{SC-CC}, defined as follows:

$$\Delta t^{SC-CC} = t^{SC} - t^{CC} - \frac{l^{SC} - l^{CC}}{c\beta} \quad , \tag{6}$$

where t^{SC} and t^{CC} are hit times, l^{SC} and l^{CC} are the path lengths from the CLAS center to the hit points in the SC and CC, and β is the track velocity measured in the SC. The distribution of SC-CC time-offsets is shown in Fig. 3. The electron-rich events outside the single photo-electron peak are emphasized by the hatched histogram, and the cut applied is shown by the dashed line. The presence of the double peak near $\Delta t^{SC-CC} \approx 0$ is expected due to a small time offset between the two PMTs within the CC segment;

6. The measured photo-electron distribution for the electron candidate events was compared to the one obtained after all the cuts described above had been applied. This comparison is shown by different histograms in Fig. 4.

After applying the matching procedure, the pion contamination was reduced from 30% to 5% in the worst case. The remaining contamination is due to events where the pion impact point in the CC is very close to the PMT with the noise signal. This contribution was removed by the same procedure as in Ref. [4]. In order to estimate the systematic uncertainties of this correction we compared the method to another approach, namely, requiring more than 2.5 photo-electrons in the CC and estimating the number of missing electrons by an extrapolation, using the empirical function from Ref. [30] adjusted for each particular run period. The difference between the two methods provides an estimate of the systematic uncertainties in the photo-electron corrections. The total relative systematic uncertainty of this correction is kinematic dependent; at larger Q^2 the contribution of pions and the corresponding systematic uncertainty are larger.

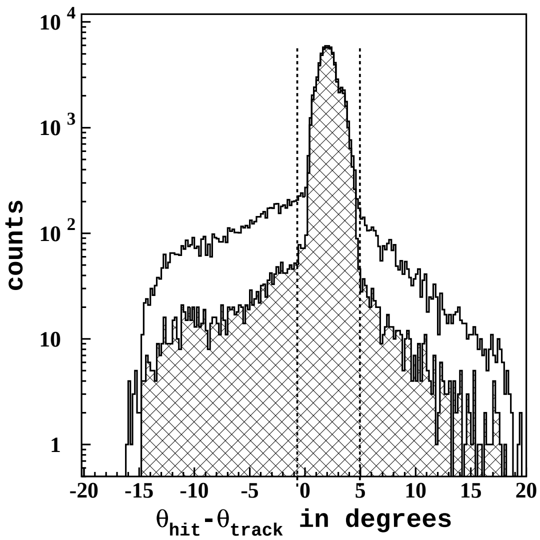

FIG. 2: The difference in the projective polar angle θ between the hit position in the CC and the impact point of the electron candidate track. The hatched area shows events with reduced pion contamination in the electron candidate sample. The reduction of the pion contamination is obtained through an additional cut: the number of photo-electrons in the CC > 2.5.

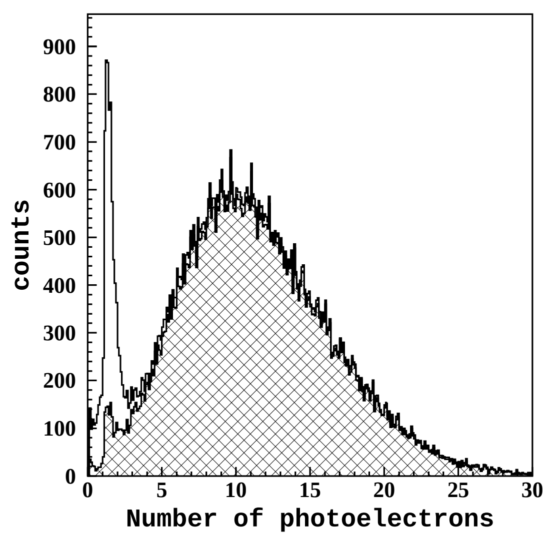

FIG. 4: The spectrum of photo-electrons measured in the CC. The hatched area represents the CC spectrum after applying the matching cuts described in the text.

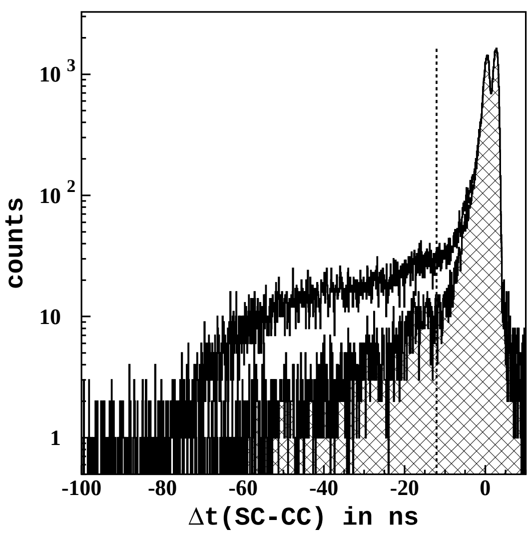

FIG. 3: The time difference between hits in the SC and the CC assigned to the electron candidate track, corrected for the distance traveled from the SC to the CC. The meaning of the two histograms is the same as in Fig. 2.

B. e^+e^- pair production

The most important source of e^+e^- pairs in the CLAS is π^0 production followed either by Dalitz decay to γe^+e^- or by $\gamma\gamma$ decay with one of the photons converting to e^+e^-. For the data set at higher beam energy some measurements were taken with an out-bending torus field[3]. This provides the possibility to extract the contribution of e^+e^- pair production directly from the data. To do so, we demanded the first particle in each event to be a positron (positron trigger), i.e. to have positive charge and hits in both the CC and the EC. We applied exactly the same cuts and corrections described above and in Ref. [4] to the positron trigger data. Following the procedure described in Ref. [31] an additional severe cut on the number of photo-electrons measured in the CC was applied ($N_{phe} > 4$) to both the electron and the positron trigger rates. The ratio e^+/e^- obtained in this way is shown in Fig. 5 in comparison with calculations described below. For the higher beam energy data set we therefore subtracted the measured e^+e^- background accounting for the statistical uncertainties only.

Since positron data are not available for the lower energy data set, the pair production background processes were estimated according to a model developed by P. Bosted and described in Ref. [31]. Bosted developed a computer code based on the Wiser fit of inclusive pion production. This model was carefully checked against other CLAS data [31], and it appeared to be in good agreement with measured positron cross sections. The value of the correction is assumed to be equal to the ratio of the inclusive e^+ production cross section over the fit of the deuteron inclusive cross section σ^M_{rad}, including radiative processes (the tail from the elastic and quasi-elastic peaks, bremsstrahlung and the Schwinger

[3] Normal setting of the CLAS torus magnet bends electrons in the forward direction along the beam (i.e. in-bending). The inverse magnetic field configuration is called out-bending.

correction). This correction factor is given by:

$$F_{e^+e^-}(E,x,Q^2) = \frac{\sigma^M_{rad}(E,x,Q^2)}{\sigma^M_{rad}(E,x,Q^2)+\sigma_{e^+}(E,x,Q^2)} \quad , \tag{7}$$

where σ_{e^+} is the inclusive e^+ production cross section and σ^M_{rad} is the fit folded with radiative processes. The index "M" here refers to the model cross section used in the event generator.

To estimate systematic uncertainties in the calculations, we compared the calculated e^+e^--pair production contribution to the measured one for the higher beam energy data. The difference, shown in Fig. 5, has been parameterized as a function of $y = \nu/E$ and is given by:

$$\delta^{e^+e^-} = 0.16 \exp\left\{-\frac{1}{2}\left(\frac{x-1}{0.1}\right)^2\right\} \quad , \tag{8}$$

where E is the beam energy and ν is the energy of the virtual photon in the Lab frame. The systematic uncertainty estimated for the lower beam energy does not exceed 3.5%.

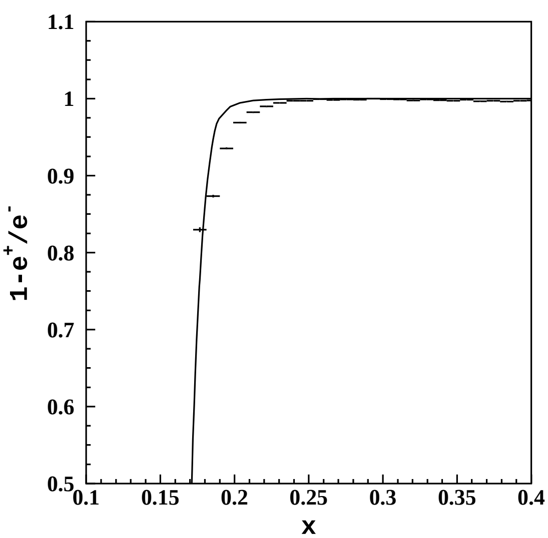

FIG. 5: The contribution of e^+e^- pair production events in the inclusive cross section at $Q^2 = 1.775$ (GeV/c)^2. The points show the measured quantity $1 - e^+/e^-$, which represents the number of electrons inelastically scattered off deuterium to the total number of measured electrons. The curve represents the calculations from Ref. [31].

C. Simulations

The simulations of the detector response were performed in the same way as described in Ref. [4]. The following improvements and changes for electron-deuteron scattering were implemented:

1. Electron scattering events were generated by a random event generator with the probability distributed according to σ^D_{rad}, described in Appendix. A. The values for the elastic and inelastic cross sections for electron-deuteron scattering were taken from existing fits of world data, in references [32] and [6], respectively. The contribution from internal radiative processes was added according to calculations [33].

2. The event rate obtained in the simulations was then compared to the data, preserving the original normalizations (accumulated Faraday Cup (FC) charge for the data and the number of generated events over the integrated cross section of the event generator for simulations). These normalized yields do not include acceptance, efficiency and radiative corrections. The simulated events passed all cuts: the fiducial cuts, calorimeter cut, event status cut (see Ref. [4] for details) and CC matching cut. However, e^+e^- pair production and empty target backgrounds were subtracted from the data. The normalized yield obtained with the same set of cuts from the data and simulations were compared and found to be in good agreement within $\approx 10-15\%$ (see Fig. 6), which is at the level of reliability for our cross section models. As one can see below in this section, a $\approx 10-15\%$ variation of the cross section model in the event generator yields only $\approx 1\%$ uncertainty in the final cross section.

In order to check the absolute normalization of the inclusive e^-D events, we used elastic e^-D scattering data. The elastic e^-D scattering cross section is well known at low Q^2 [34]. We performed the simulations of this reaction using the parameterization from Ref. [34]. The normalized event yield obtained from simulations ($\frac{d\sigma}{d\Omega}_{sim}$) was compared to the measured one ($\frac{d\sigma}{d\Omega}_{exp}$) at the lowest Q^2 values. The two yields are in good agreement within statistical and systematic uncertainties as shown in Fig. 7. The distortion of the measured peak is due to radiative corrections not taken into account in the simulations. The efficiency obtained from simulations and checked against the elastic scattering data appear to be approximately constant (about 90-95%) inside the fiducial region of the detector defined by the fiducial cuts.

The elastic scattering normalized yield was evaluated as the number of e^-D coincidences measured in CLAS in the $W_D = \sqrt{M_D^2 + 2M_D\nu - Q^2}$-interval from 1.75 to 2 GeV multiplied by the corresponding luminosity:

$$\frac{d\sigma}{d\Omega}_{exp,sim}(E,\theta) = \frac{L_{sim}}{\rho \frac{N_A}{M_A} L Q_{tot}} \int_{1.75}^{2} dW_D N_{exp,sim}(W_D,\theta) \quad , \tag{9}$$

where $N_{exp,sim}$ represents the corresponding numbers of events (for the measured cross section the empty target events were subtracted). In order to clean up the elastic data sample, we applied additional cuts on the deuteron identification $|M_D^{2\,(exp)} - M_D^2| < 0.5$ GeV^2 and the kine-

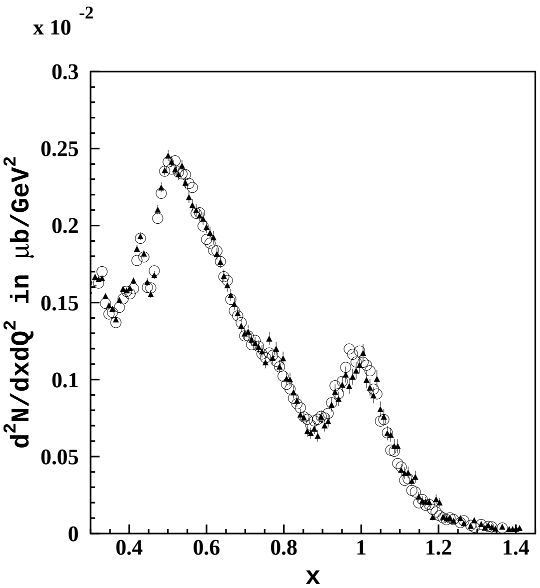

FIG. 6: The normalized event yield obtained from the data (open circles) and simulations (filled triangles) at $E = 5.77$ GeV, $Q^2 = 2.425$ (GeV/c)^2. The yields were obtained within fiducial and EC cuts. An e^+e^- correction was applied to the data. No acceptance or efficiency was applied to either spectrum.

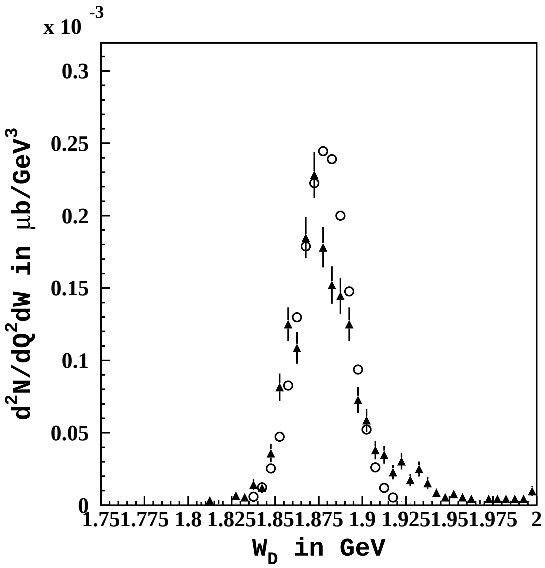

FIG. 7: Normalized yield of elastic electron scattering off the deuteron at $Q^2 = 0.47 - 0.63$ (GeV/c)^2: the data are shown by the open circles and the simulations are shown by the triangles. No acceptance or efficiency corrections were applied.

matic correlations between the electron and deuteron:

$$||\phi_e - \phi_D| - 180^\circ| < 3^\circ \text{ and } \tag{10}$$
$$\left|\cos\theta_D - \frac{(E_0 - P_e\cos\theta_e)}{P_D}\right| < 0.1 \quad ,$$

where $M_D^{(exp)}$ is the mass of the deuteron measured in the SC; M_D is the nominal deuteron mass; ϕ_e (θ_e) and ϕ_D (θ_D) represent the azimuthal (polar) angles (in degrees) of the scattered electron and deuteron, respectively; P_e and P_D are the momenta of the particles. As one can see from Fig. 7 the elastic peak is very well separated from the inelastic background and some distortion of the peak in the data is due to radiative effects. The integrated peak cross sections agree to within the 3% statistical uncertainty.

There are two systematic uncertainties in the simulation. The first one is due to the model dependence of the reaction cross section used for generating the events. We applied a different cross section model for the inelastic electron-deuteron scattering, taken from Ref. [35], and the differences obtained for the efficiency were taken as an estimate of the systematic uncertainty. These systematic uncertainties were averaged over both kinematic variables to give a uniform systematic uncertainty to both data sets, which was estimated to be 1.7%. The second systematic uncertainty is due to the inability of the GEANT3-based CLAS simulation package GSIM [36] to perfectly reproduce the CLAS response to electron tracks at different angles and momenta. To estimate this effect, we treated the six CLAS sectors as independent spectrometers. The normalized event yield measured in each sector was compared separately to the simulations, as shown in Fig. 6. The observed differences were compared sector-by-sector to remove uncertainties due to the event generator model. From this comparison we obtained a systematic uncertainty varying from 3 to 6% depending mostly on the scattered electron polar angle. The two uncertainties were summed in quadrature.

D. Structure Function $F_2(x, Q^2)$

The measured electron yields N_{exp}, normalized to the integrated luminosity in conjunction with Monte Carlo simulations, were used to extract the structure function F_2 in each kinematic bin. The Monte Carlo events were used to simultaneously obtain efficiency, acceptance, bin centering and radiative corrections. F_2 was determined using:

$$F_2(x, Q^2) = \frac{1}{\rho\frac{N_A}{M_A}LQ_{tot}} \frac{J}{\sigma_{Mott}} \frac{\nu}{1 + \frac{1-\epsilon}{\epsilon}\frac{1}{1+R}} \frac{N_{exp}(x, Q^2)}{\Psi(x, Q^2)} F_{phe}(x, Q^2) F_{e^+e^-}(x, Q^2) \; , \tag{11}$$

where ρ is the density of liquid D_2 in the target, N_A is the Avogadro constant, M_A is the target molar mass, L is the target length, Q_{tot} is the total charge in the Faraday Cup (FC) and $\Psi(x, Q^2)$ is the efficiency including the radiative and bin-centering correction factors:

$$\Psi(x, Q^2) = \Psi_{eff}(x, Q^2)\Psi_{rad}(x, Q^2)\Psi_{bin}(x, Q^2) \; , \tag{12}$$

with:

$$\Psi_{rad} = \frac{\sigma^M_{rad}}{\sigma^M} \quad \text{and} \quad \Psi_{bin} = \frac{\int_{\Delta\tau} d\sigma^M}{\sigma^M} \; , \tag{13}$$

Ψ_{eff} is the ratio between the number of reconstructed and generated events in the bin. The integral in Eq. 13 was taken over the current bin area $\Delta\tau$. Here ϵ is the virtual photon polarization parameter:

$$\epsilon \equiv \left(1 + 2\frac{\nu^2 + Q^2}{Q^2}\tan^2\frac{\theta}{2}\right)^{-1} . \quad (14)$$

The Mott cross section σ_{Mott} and the Jacobian J of the transformation between $d\Omega dE'$ to $dxdQ^2$ are defined by:

$$\sigma_{Mott} = \frac{\alpha^2 \cos^2\frac{\theta}{2}}{4E^2 \sin^4\frac{\theta}{2}} \quad \text{and} \quad J = \frac{xEE'}{\pi\nu} . \quad (15)$$

The structure function $F_2(x, Q^2)$ was extracted using the fit of the function $R(x, Q^2) \equiv \sigma_L/\sigma_T$ described in Appendix B. However, the structure function F_2 in the relevant kinematic range is very insensitive to the value of R.

Fig. 8 shows a comparison between the F_2 data from CLAS and the other world data in the Q^2 =1.825 (GeV/c)^2 bin. The CLAS data agree very well with all previous measurements. The values of $F_2(x, Q^2)$, together with their statistical and systematic uncertainties, are tabulated elsewhere [37].

In the calculation of the radiative correction factor Ψ_{rad} we used the cross section model described in Appendix A in the following way:

- the eD elastic radiative tail was calculated according to the "exact" Mo and Tsai formula [33];

- in the quasi-elastic peak region ($W^{el} + \Delta W < W <$ 1.2 GeV) we applied the correction formula to the continuum spectrum given in Ref. [33], which is based on the peaking approximation and is known to be reliable only when $E'/E > 0.5$. Here W^{el} is the eD elastic peak position and ΔW its width;

- at $W > 1.2$ GeV we applied the exact Mo and Tsai formula also to the quasi-elastic tail and a peaking approximation based formula (referred to as the "unfolding procedure") to the inelastic spectrum. For an exact calculation of the quasi-elastic tail it was necessary to extract quasi-elastic form-factors. To this end we integrated the quasi-elastic cross section from the beginning of the peak up to $W = 1.2$ GeV and performed a separation of the electric and magnetic form-factors. These two kinematic regions overlap quite well and don't exhibit any discontinuity at the point $W = 1.2$ GeV. This assured us that the peaking approximation formalism is safely applicable to the quasi-elastic tail up to $W = 1.2$ GeV.

The radiative correction factor Ψ_{rad} varies strongly in the explored kinematic range from 0.7 up to 1.5. Fortunately, the largest corrections are given by the tails of the elastic and quasi-elastic peaks, for which calculations are very accurate (see Refs. [33, 38]). The largest systematic uncertainties (see Table I) are due to the efficiency evaluation, and to the photo-electron and radiative corrections.

The systematic uncertainties for the efficiency evaluation, the e^+e^- pair correction, and the photo-electron correction were described above, and the systematic uncertainties arising from the applied CLAS momentum correction routines are calculated according to Ref. [4]. The radiative correction factors in σ^M_{rad} were evaluated with two different methods ([33], [38]) and the difference was taken as an estimate of the corresponding systematic uncertainty. These two methods use different parameterizations of the elastic ([32] and [38]), quasi-elastic ([35] and [38]) and inelastic ([6] and [38]) cross sections, as well as different calculation techniques. The uncertainties in R given in Appendix B were propagated to the resulting F_2. All systematic uncertainties were summed in quadrature to obtain the final systematic uncertainty.

The statistical and systematic precisions of the extracted structure function F_2 are strongly dependent on the kinematics: the statistical uncertainties vary from 0.1% up to 30% at the largest Q^2, where the event yield is very limited, while the average value is about 3%; the systematic uncertainties range from 4% up to 14%, with the mean value being about 7% (see Table I).

TABLE I: Range and average of systematic uncertainties on F_2.

Source of uncertainties	Variation range	Average
	[%]	[%]
Efficiency evaluation	3-7	4.6
e^+e^- pair production correction	0-3	0.1
Photoelectron correction	0.1-6	2.4
Radiative correction	1.8-3.5	2.3
Momentum correction	0.2-1.2	0.5
Uncertainty of $R = \frac{\sigma_L}{\sigma_T}$	0.2-0.75	0.5
Empty target subtraction	0.4-0.42	0.4
Total	4-14	6.6

E. Moments of the Structure Function F_2

The evaluation of the deuteron structure function moments was performed according to the method developed in Ref. [4]. However, there are two main differences in the deuteron data analysis:

1. the quasi-elastic peak is not as well known as the proton elastic form-factors, and moreover cannot be easily separated from the inelastic spectrum. Hence, in contrast to the free proton target, we extract the total moments of the deuteron structure function F_2 directly, without separating them into the elastic and inelastic parts. This emphasizes the

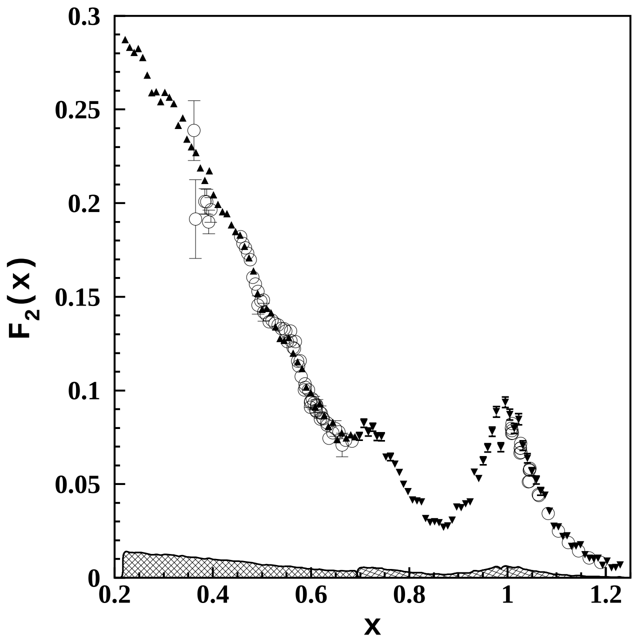

FIG. 8: The deuteron structure function $F_2(x, Q^2)$ per nucleon at $Q^2 = 1.825$ (GeV/c)^2. The triangles represent experimental data obtained in the present analysis with systematic uncertainties indicated by the hatched area. The empty circles show data from previous experiments [6, 7, 8, 9, 10, 11, 12, 13, 14, 15].

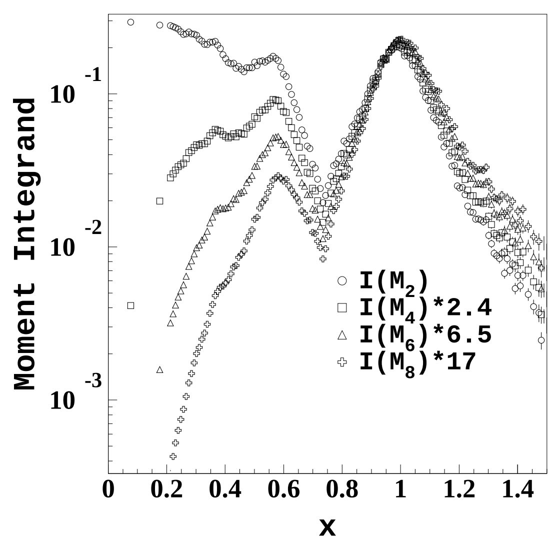

FIG. 9: Integrands of the Nachtmann moments at $Q^2 = 0.825$ (GeV/c)^2: circles represent the integrand of the M_2; squares show the integrand of the M_4; triangles show the integrand of the M_6; crosses show the integrand of the M_8.

importance of a precise determination of the quasi-elastic peak for each Q^2 together with the inelastic spectrum. In particular, the contribution of the quasi-elastic peak in the higher moments ($n > 2$) at Q^2 values in the interval 1-5 (GeV/c)^2 is very significant, as one can see in Fig. 9. Thanks to the high precision of the CLAS data this problem is well addressed now;

2. the lack of collider data does not allow one to reach very low x values. For the second moment M_2 this leads to an increase of systematic uncertainties due to the low-x extrapolation with respect to the proton M_2. The contribution of the low x part in the higher moments however is negligible. We used two models of the deuteron structure function F_2 which have very different low-x behaviour to estimate the extrapolated part of the second moment M_2. The difference between the two estimates was taken as an evaluation of the corresponding systematic uncertainty. A comparison of the extrapolation systematic uncertainties and other uncertainties in M_2 is shown in Fig. 10.

We combined the structure functions F_2 obtained from the CLAS data and the other world data on the structure function F_2, along with the inclusive cross section data from Refs. [6, 7, 8, 9, 10, 11, 12, 13, 14, 15, 16, 17, 18, 19, 20] (see Fig. 1). The data from Ref. [39], recently reanalyzed in Ref. [40] with the inclusion of radiative and bin centering corrections, are not used in the present analysis due to large statistical uncertainties and unknown systematic uncertainties. The Q^2-range of the CLAS data, from 0.4 to 5.95 (GeV/c)^2, was divided into bins of width $\Delta Q^2 = 0.05$ (GeV/c)^2. Within each Q^2 bin the world data were shifted to the central bin value Q_0^2, using the fit of $F_2^M(x, Q^2)$ from Appendix. A. The integrals of the data over x were performed numerically using the standard trapezoidal method TRAPER [41]. As an example, Fig. 9 shows the integrands of the first four moments as a function of x at fixed Q^2. The significance of the large x region for various moments can clearly be seen.

As in Ref. [4], the world data at Q^2 above 6 (GeV/c)^2 were analyzed in the same way as described above, but with a different Q^2 bin size. The bin size was chosen for the data to provide sufficient x-coverage for most of the Q^2 bins ($\Delta Q^2/Q^2 = 5$ %). The results together with their statistical and systematic uncertainties are shown in Fig. 11 and reported in Table II.

The systematic uncertainty consists of experimental uncertainties in the data given in Refs. [6, 7, 8, 9, 10, 11, 12, 13, 14, 15, 16, 17, 18, 19, 20] and uncertainties in the evaluation procedure. To estimate the first type of uncertainty we had to account for the inclusion of many data sets measured in different laboratories with different detectors. In the present analysis we assume that the different experiments are independent and therefore only the systematic uncertainties within a given data set are correlated.

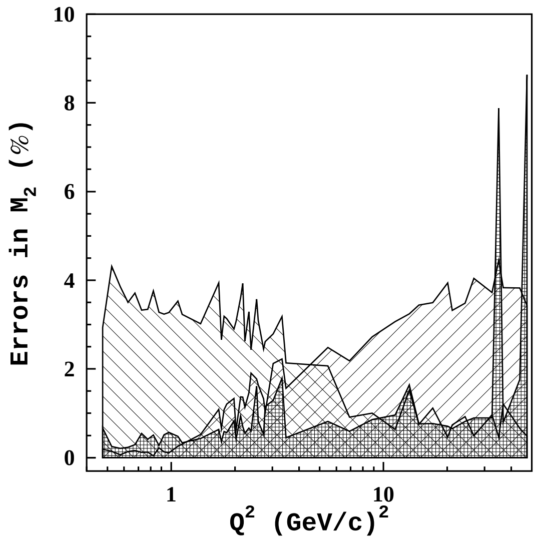

FIG. 10: Uncertainties of the Nachtmann moment M_2 in percentage. The lower cross-hatched area represents statistical uncertainties. The left-hatched area represents the systematic uncertainties. The right-hatched area represents the low-x extrapolation uncertainty.

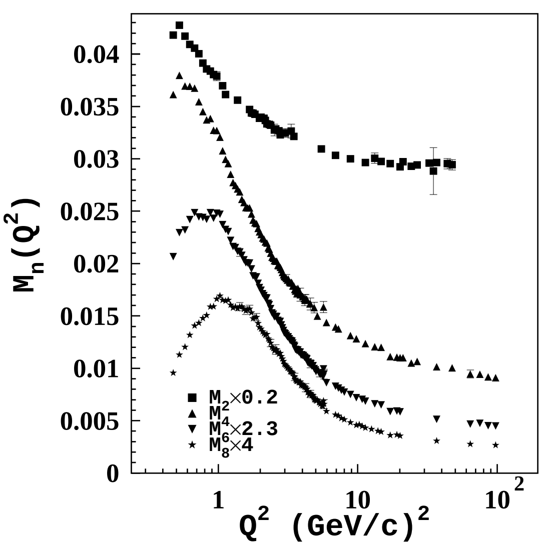

FIG. 11: The Nachtman moments extracted from the world data, including the new CLAS results. Uncertainties are statistical only.

IV. SEPARATION OF LEADING AND HIGHER TWISTS

In order to separate the leading and higher twists in the measured moments we used the method developed in Refs. [4, 23, 42]. This method is essentially based on a general form of the OPE for the structure function moments, where the leading twist Q^2-evolution is calculated in pQCD and the deviation from this behaviour is assigned to the higher twist contribution. Therefore the measured Nachtmann n-th moment was parameterized as:

$$M_n^N(Q^2) = \eta_n(Q^2) + HT_n(Q^2) \ , \tag{16}$$

where $\eta_n(Q^2)$ is the leading twist moment and $HT_n(Q^2)$ is the higher twist contribution. The leading twist term was calculated at NLO including gluon re-summation (SGR) corrections which take into account the rest of the pQCD series beyond NLO. The observed decoupling of the singlet quark and gluon densities at large x [42] allows us to consider only the non-singlet (NS) evolution for $n \geq 4$ and therefore to reduce the number of leading twist parameters. In this approximation the leading twist moment $\eta_n(Q^2)$ for $n \geq 4$ can be written as follows:

$$\begin{aligned}\eta_n(Q^2) \ = \ & A_n \left[\frac{\alpha_s(Q^2)}{\alpha_s(\mu^2)}\right]^{\gamma_n^{NS}} \\ & \left\{ \left[1 + \frac{\alpha_s(Q^2)}{2\pi} C_{DIS}^{(NLO)}\right] e^{G_n(Q^2)} + \right. \\ & \left. \frac{\alpha_s(Q^2)}{4\pi} R_n^{NS} \right\} \ , \end{aligned} \tag{17}$$

where the quantities γ_n^{NS}, $C_{DIS}^{(NLO)}$ and R_n^{NS} can be obtained from Ref. [23], $\alpha_s(M_Z^2) = 0.118$ [43] and the reference scale $\mu^2 = 10$ (GeV/c)^2. In Eq. 17 the function $G_n(Q^2)$ is the key quantity of the soft gluon resummation. At Next-to-Leading-Log it reads as:

$$G_n(Q^2) = \ln(n) G_1(\lambda_n) + G_2(\lambda_n) + O[\alpha_s^k \ln^{k-1}(n)] \ , \tag{18}$$

where $\lambda_n \equiv \beta_0 \alpha_s(Q^2) \ln(n)/4\pi$ and:

$$\begin{aligned} G_1(\lambda) \ &= \ C_F \frac{4}{\beta_0 \lambda} \left[\lambda + (1-\lambda)\ln(1-\lambda)\right] \ , \\ G_2(\lambda) \ &= \ -C_F \frac{4\gamma_E + 3}{\beta_0} \ln(1-\lambda) \\ & \quad - C_F \frac{8K}{\beta_0^2} \left[\lambda + \ln(1-\lambda)\right] \\ & \quad + C_F \frac{4\beta_1}{\beta_0^3} \left[\lambda + \ln(1-\lambda) + \frac{1}{2}\ln^2(1-\lambda)\right] \ , \end{aligned} \tag{19}$$

with $C_F \equiv (N_c^2 - 1)/(2N_c)$, $k = N_c(67/18 - \pi^2/6) - 5N_f/9$, $\beta_0 = 11 - 2N_f/3$, and N_f being the number of active flavors. Note that the function $G_2(\lambda)$ is divergent for $\lambda \to 1$. This means that at large n (i.e. large x) the soft gluon re-summation cannot be extended to arbitrarily low values of Q^2. Therefore, for a safe use of present SGR techniques we work far from the above-mentioned divergences by limiting our analysis of low-order moments ($n \leq 8$) to $Q^2 \geq 0.7 - 1$ (GeV/c)^2.

Since a complete calculation of the higher twist anomalous dimensions is not yet available, we use the same phenomenological ansatz already adopted in Refs. [4, 23, 42]. In this approach the higher twist contribution is given by [44]:

$$HT_n(Q^2) = a_n^{(4)} \left[\frac{\alpha_s(Q^2)}{\alpha_s(\mu^2)}\right]^{\gamma_n^{(4)}} \frac{\mu^2}{Q^2} + a_n^{(6)} \left[\frac{\alpha_s(Q^2)}{\alpha_s(\mu^2)}\right]^{\gamma_n^{(6)}} \frac{\mu^4}{Q^4} , \quad (20)$$

where the logarithmic pQCD evolution of the twist-τ contribution is accounted for by the term $[\alpha_s(Q^2)/\alpha_s(\mu^2)]^{\gamma_n^{(\tau)}}$. This term corresponds to the Wilson coefficient $E_{n\tau}(\mu_r, \mu_f, Q^2)$ in Eq. 2 with an *effective* anomalous dimension $\gamma_n^{(\tau)}$. The parameter $a_n^{(\tau)}$ represents the overall strength of the twist-τ term at the renormalization scale $Q^2 = \mu^2$ and it is proportional to the matrix element $O_{n\tau}(\mu)$ in Eq. 2. The presence of two distinct higher twist terms for $n \geq 4$ is motivated by the Q^2-behaviour of the total higher twist contribution in the moments. This was obtained by a direct subtraction of the leading twist term fitted to the large Q^2 part of the plot from the measured moments. Existence of maxima and moreover of the sign turn-over (see Fig. 12) in the total higher twist contribution cannot be described by a single twist term within the pQCD-inspired model from Eq. 20. Therefore, the presence of at least two higher twist terms is necessary for a successful description of experimental data. We checked that the variation of the total higher twist contribution after inclusion of twist-8 and twist-10 terms is smaller than the quoted systematic uncertainties.

The n-th moment (see Eqs. 16, 17 and 20) for $n \geq 4$ has five unknown parameters: the twist-2 parameter A_n, which represents the value of the leading twist moment at $Q^2 = \mu^2$, and the higher twist parameters $a_n^{(4)}, \gamma_n^{(4)}, a_n^{(6)}, \gamma_n^{(6)}$. All five unknown parameters were simultaneously determined from a χ^2-minimization procedure in the Q^2 range between 1 and 100 (GeV/c)^2. In this procedure only the statistical uncertainties of the experimental moments were taken into account. The uncertainties of the various twist parameters were then obtained by adding the systematic uncertainties to the experimental moments and by repeating the twist extraction procedure.

For $n = 2$, $\eta_2(Q^2)$ is given by the sum of the non-singlet and singlet terms, which yield two unknown parameters associated with the leading twist. These parameters are the values of the gluon and non-singlet quark moments at the factorization scale $Q^2 = \mu^2$. However, due to the vanishing contribution of the higher twists in M_2 (see Fig. 12) one can reduce the number of parameters in $HT_n(Q^2)$ by limiting the expansion to the twist-4 term only.

The parameter values obtained at the renormalization scale $\mu^2 = 10$ (GeV/c)^2 are reported in Table III, where it can be seen that the leading twist is determined with an uncertainty of a few percent, while the precision of the extracted higher twists decreases with n, reaching an overall 20-30% for $n = 8$, thanks to the remarkable quality of the CLAS data at large x. Note that the leading twist is directly extracted from the data, which means that no specific functional shape of the parton distributions is assumed in our analysis.

Our results for each twist term are reported in Fig. 12 for $n \geq 2$, while the ratio of the total higher twist contribution to the leading twist is shown in Fig. 13. In addition, the extracted leading twist contribution is reported in Table IV.

V. CONCLUSIONS

We extracted the deuteron F_2 structure function in a continuous two-dimensional range of Q^2 and x from the inclusive cross sections measured with CLAS. The extracted structure functions are in good agreement with previous measurements in overlapping regions, contribute many additional kinematic points and improve the precision where the world data exist. Using these data, together with the previously available world data set, we evaluated for the first time the Nachtmann moments $M_2(Q^2, x)$, $M_4(Q^2, x)$, $M_6(Q^2, x)$ and $M_8(Q^2, x)$ in the Q^2 range $0.5 - 100$ (GeV/c)^2. Previously, the experimental information on the deuteron structure function moments was missing in the low to medium Q^2 domain due to scarce data at $x \rightarrow 1$. Moreover, fixed Q^2 bins of the data allowed us to reduce dramatically the uncertainties of the moment evaluation procedure, rendering the Q^2-evolution of the extracted moments model-independent. The measured moments have been analyzed in terms of a twist expansion in order to extract both the leading and the higher twists simultaneously. By calculating the Q^2-evolution of the leading twist at NLO and including α_S-higher order corrections through the soft gluon re-summation, we extracted values of the reduced matrix elements O_{n2} from Eq. 2. higher twists have been treated phenomenologically within the pQCD-inspired approach of Eq. 20 by introducing *effective* anomalous dimensions. The Q^2 interval of the analysis was quite large, ranging from 1 to 100 (GeV/c)^2, allowing us to determine the total contribution of higher twists to the best accuracy possible. The variation of the total higher twist contribution due to inclusion of twist-8 and twist-10 terms is lower than the quoted systematic uncertainties. The leading twist is determined with a few percent uncertainty, while the precision of the higher twists decreases with n reaching an overall 20-30% for n =8, thanks to the remarkable quality of the experimental moments.

The main results of our twist analysis can be summarized as follows:

- the extracted leading term yields the dominant contribution in the entire Q^2-range of the present analysis for all four moments. This leads to the conclusion that despite the nuclear effects, a pQCD-based description of the deuteron structure is surprisingly

TABLE II: The Nachtmann moments for $n = 2, 4, 6$ and 8 evaluated in the interval $0.05 \leq\ Q^2 \leq 100$ (GeV/c)^2. The moments are labeled with an asterisk when the contribution to the integral by the experimental data is between 50% and 70%. All the others were evaluated with more than 70% data coverage. The data are reported together with the statistical and systematic uncertainties.

Q^2 [(GeV/c)^2]	$M_2(Q^2)$x10^{-1}	$M_4(Q^2)$x10^{-2}	$M_6(Q^2)$x10^{-2}	$M_8(Q^2)$x10^{-3}
0.475	2.133 ± 0.014 ± 0.063	3.673 ± 0.035 ± 0.139	0.911 ± 0.010 ± 0.037	2.421 ± 0.030 ± 0.101
0.525	2.168 ± 0.005 ± 0.093	3.868 ± 0.017 ± 0.171	1.011 ± 0.005 ± 0.046	2.852 ± 0.016 ± 0.129
0.575	2.118 ± 0.004 ± 0.082	3.776 ± 0.011 ± 0.168	1.026 ± 0.004 ± 0.047	3.042 ± 0.012 ± 0.140
0.625	2.084 ± 0.005 ± 0.073	3.757 ± 0.008 ± 0.162	1.067 ± 0.003 ± 0.048	3.328 ± 0.010 ± 0.154
0.675	2.064 ± 0.006 ± 0.077	3.757 ± 0.009 ± 0.179	1.101 ± 0.003 ± 0.053	3.572 ± 0.013 ± 0.172
0.725	2.027 ± 0.011 ± 0.067	3.632 ± 0.010 ± 0.168	1.086 ± 0.004 ± 0.053	3.641 ± 0.016 ± 0.178
0.775	1.970 ± 0.008 ± 0.066	3.515 ± 0.012 ± 0.155	1.080 ± 0.005 ± 0.051	3.752 ± 0.022 ± 0.182
0.825	1.955 ± 0.010 ± 0.073	3.460 ± 0.012 ± 0.174	1.079 ± 0.005 ± 0.055	3.840 ± 0.024 ± 0.195
0.875	1.968 ± 0.005 ± 0.064	3.474 ± 0.007 ± 0.175	1.108 ± 0.003 ± 0.058	4.056 ± 0.015 ± 0.213
0.925	1.926 ± 0.010 ± 0.062	3.357 ± 0.014 ± 0.166	1.082 ± 0.007 ± 0.057	4.042 ± 0.035 ± 0.213
0.975	1.916 ± 0.011 ± 0.063	3.352 ± 0.013 ± 0.162	1.106 ± 0.006 ± 0.058	4.238 ± 0.032 ± 0.225
1.025		3.280 ± 0.013 ± 0.169	1.099 ± 0.006 ± 0.060	4.320 ± 0.034 ± 0.239
1.075	1.873 ± 0.009 ± 0.066	3.159 ± 0.014 ± 0.164	1.059 ± 0.007 ± 0.059	4.215 ± 0.039 ± 0.240
1.125	1.837 ± 0.006 ± 0.059	3.071 ± 0.007 ± 0.147	1.036 ± 0.003 ± 0.056	4.190 ± 0.018 ± 0.235
1.175		3.012 ± 0.008 ± 0.132	1.022 ± 0.003 ± 0.052	4.201 ± 0.017 ± 0.228
1.225		2.934 ± 0.016 ± 0.148	0.997 ± 0.007 ± 0.055	4.136 ± 0.037 ± 0.234
1.275		2.842 ± 0.013 ± 0.147	0.965 ± 0.006 ± 0.053	4.035 ± 0.032 ± 0.230
1.325		2.809 ± 0.012 ± 0.154	0.961 ± 0.005 ± 0.055	4.080 ± 0.027 ± 0.238
1.375	1.807 ± 0.008 ± 0.055	2.789 ± 0.014 ± 0.138	0.951 ± 0.008 ± 0.053	4.064 ± 0.046 ± 0.238
1.425		2.751 ± 0.011 ± 0.130	0.944 ± 0.006 ± 0.051	4.086 ± 0.033 ± 0.235
1.475		2.681 ± 0.016 ± 0.119	0.926 ± 0.007 ± 0.047	4.063 ± 0.041 ± 0.221
1.525		2.636 ± 0.015 ± 0.149	0.906 ± 0.007 ± 0.052	3.993 ± 0.041 ± 0.232
1.575		2.574 ± 0.014 ± 0.153	0.891 ± 0.007 ± 0.056	3.956 ± 0.043 ± 0.252
1.625		2.582 ± 0.011 ± 0.140	0.894 ± 0.005 ± 0.052	3.992 ± 0.025 ± 0.236
1.675	1.745 ± 0.011 ± 0.069	2.575 ± 0.013 ± 0.135	0.891 ± 0.007 ± 0.051	4.012 ± 0.042 ± 0.239
1.725	1.733 ± 0.006 ± 0.046	2.527 ± 0.008 ± 0.115	0.872 ± 0.005 ± 0.046	3.942 ± 0.033 ± 0.225
1.775	1.721 ± 0.010 ± 0.055	2.468 ± 0.009 ± 0.109	0.845 ± 0.006 ± 0.041	3.816 ± 0.035 ± 0.200
1.825	1.709 ± 0.010 ± 0.054	2.413 ± 0.010 ± 0.111	0.829 ± 0.007 ± 0.041	3.789 ± 0.048 ± 0.193
1.875		2.402 ± 0.013 ± 0.117	0.824 ± 0.006 ± 0.045	3.774 ± 0.031 ± 0.212
1.925		2.349 ± 0.018 ± 0.112	0.794 ± 0.008 ± 0.041	3.610 ± 0.047 ± 0.200
1.975	1.697 ± 0.014 ± 0.049	2.315 ± 0.012 ± 0.105	0.777 ± 0.008 ± 0.039	3.519 ± 0.060 ± 0.186
2.025	1.698 ± 0.007 ± 0.052	2.280 ± 0.005 ± 0.106	0.762 ± 0.003 ± 0.038	3.456 ± 0.018 ± 0.178
2.075		2.246 ± 0.011 ± 0.104	0.747 ± 0.004 ± 0.037	3.395 ± 0.023 ± 0.171
2.125	1.696 ± 0.016 ± 0.061	2.244 ± 0.010 ± 0.110	0.744 ± 0.007 ± 0.038	3.383 ± 0.054 ± 0.172
2.175	1.684 ± 0.012 ± 0.066	2.211 ± 0.010 ± 0.109	0.731 ± 0.007 ± 0.037	3.324 ± 0.052 ± 0.172
2.225	1.687 ± 0.009 ± 0.044	2.201 ± 0.004 ± 0.103	0.728 ± 0.002 ± 0.036	3.324 ± 0.016 ± 0.168
2.275		2.168 ± 0.019 ± 0.099	0.716 ± 0.004 ± 0.035	3.274 ± 0.023 ± 0.162
2.325	1.683 ± 0.011 ± 0.055	2.148 ± 0.006 ± 0.094	0.700 ± 0.004 ± 0.032	3.179 ± 0.029 ± 0.149
2.375	1.669 ± 0.010 ± 0.041	2.104 ± 0.005 ± 0.085	0.685 ± 0.003 ± 0.030	3.121 ± 0.027 ± 0.143
2.425		2.063 ± 0.006 ± 0.088	0.666 ± 0.003 ± 0.028	3.016 ± 0.021 ± 0.130
2.475		2.054 ± 0.008 ± 0.079	0.661 ± 0.003 ± 0.027	2.991 ± 0.020 ± 0.125
2.525	1.639 ± 0.026 ± 0.059	2.034 ± 0.005 ± 0.089	0.653 ± 0.002 ± 0.028	2.956 ± 0.019 ± 0.121
2.575	1.644 ± 0.013 ± 0.051	2.032 ± 0.008 ± 0.091	0.656 ± 0.005 ± 0.032	2.990 ± 0.042 ± 0.144
2.625		2.026 ± 0.009 ± 0.101	0.652 ± 0.004 ± 0.034	2.974 ± 0.032 ± 0.153
2.675		1.986 ± 0.008 ± 0.090	0.637 ± 0.003 ± 0.032	2.914 ± 0.021 ± 0.154
2.725	1.652 ± 0.009 ± 0.040	1.990 ± 0.004 ± 0.093	0.630 ± 0.002 ± 0.032	2.865 ± 0.017 ± 0.152
2.775	1.620 ± 0.019 ± 0.042	1.961 ± 0.015 ± 0.089	0.623 ± 0.008 ± 0.032	2.819 ± 0.062 ± 0.151
2.825		1.939 ± 0.029 ± 0.092	0.613 ± 0.007 ± 0.032	2.780 ± 0.038 ± 0.149
2.875		1.912 ± 0.015 ± 0.103	0.600 ± 0.008 ± 0.031	2.707 ± 0.060 ± 0.144
2.925		1.891 ± 0.005 ± 0.090	0.591 ± 0.003 ± 0.030	2.668 ± 0.020 ± 0.139
2.975		1.896 ± 0.016 ± 0.096	0.588 ± 0.007 ± 0.032	2.641 ± 0.057 ± 0.142
3.025	1.624 ± 0.021 ± 0.045	1.873 ± 0.011 ± 0.090	0.581 ± 0.006 ± 0.032	2.607 ± 0.057 ± 0.144
3.075		1.853 ± 0.039 ± 0.090	0.571 ± 0.007 ± 0.032	2.557 ± 0.038 ± 0.145
3.125		1.851 ± 0.006 ± 0.100	0.571 ± 0.003 ± 0.032	2.566 ± 0.020 ± 0.147
3.175		1.852 ± 0.031 ± 0.110	0.567 ± 0.009 ± 0.034	2.536 ± 0.059 ± 0.149
3.225		1.823 ± 0.007 ± 0.097	0.557 ± 0.003 ± 0.032	2.482 ± 0.021 ± 0.146
3.275		1.818 ± 0.018 ± 0.098	0.551 ± 0.009 ± 0.033	2.429 ± 0.067 ± 0.144

Q^2 [(GeV/c)^2]	$M_2(Q^2)$x10^{-1}	$M_4(Q^2)$x10^{-2}	$M_6(Q^2)$x10^{-2}	$M_8(Q^2)$x10^{-3}
3.325	1.632 ± 0.029 ± 0.052	1.816 ± 0.016 ± 0.095	0.545 ± 0.008 ± 0.032	2.397 ± 0.071 ± 0.144
3.375		1.807 ± 0.017 ± 0.090	0.544 ± 0.009 ± 0.032	2.390 ± 0.069 ± 0.144
3.425		1.779 ± 0.005 ± 0.101	0.536 ± 0.003 ± 0.031	2.367 ± 0.018 ± 0.144
3.475	1.622 ± 0.007 ± 0.035	1.792 ± 0.005 ± 0.090	0.531 ± 0.002 ± 0.032	2.314 ± 0.019 ± 0.143
3.525		1.754 ± 0.023 ± 0.090	0.527 ± 0.010 ± 0.031	2.298 ± 0.067 ± 0.143
3.575		1.742 ± 0.015 ± 0.083	0.518 ± 0.003 ± 0.029	2.272 ± 0.020 ± 0.138
3.625		1.758 ± 0.030 ± 0.120	0.514 ± 0.009 ± 0.033	2.224 ± 0.054 ± 0.138
3.675		1.717 ± 0.030 ± 0.093	0.509 ± 0.005 ± 0.032	2.210 ± 0.029 ± 0.138
3.725		1.739 ± 0.030 ± 0.130	0.508 ± 0.009 ± 0.034	2.196 ± 0.060 ± 0.146
3.775		1.703 ± 0.023 ± 0.094	0.504 ± 0.005 ± 0.033	2.188 ± 0.025 ± 0.148
3.825		1.735 ± 0.006 ± 0.126	0.501 ± 0.003 ± 0.034	2.165 ± 0.025 ± 0.142
3.875		1.681 ± 0.021 ± 0.105	0.498 ± 0.003 ± 0.031	2.179 ± 0.020 ± 0.140
3.925			0.496 ± 0.009 ± 0.034	2.145 ± 0.051 ± 0.143
3.975			0.494 ± 0.002 ± 0.030	2.151 ± 0.016 ± 0.139
4.025		1.694 ± 0.031 ± 0.085	0.494 ± 0.010 ± 0.031	2.123 ± 0.066 ± 0.137
4.075			0.487 ± 0.006 ± 0.034	2.101 ± 0.030 ± 0.143
4.125		1.657 ± 0.009 ± 0.083	0.486 ± 0.003 ± 0.031	2.121 ± 0.017 ± 0.144
4.175		1.658 ± 0.062 ± 0.086	0.486 ± 0.013 ± 0.031	2.112 ± 0.073 ± 0.146
4.225		1.664 ± 0.045 ± 0.093	0.482 ± 0.014 ± 0.031	2.084 ± 0.097 ± 0.147
4.275		1.630 ± 0.030 ± 0.075	0.475 ± 0.010 ± 0.030	2.041 ± 0.066 ± 0.141
4.325		1.636 ± 0.012 ± 0.085	0.474 ± 0.003 ± 0.031	2.047 ± 0.020 ± 0.146
4.375			0.466 ± 0.007 ± 0.034	1.986 ± 0.036 ± 0.144
4.425			0.465 ± 0.008 ± 0.035	1.982 ± 0.050 ± 0.147
4.475			0.459 ± 0.005 ± 0.035	1.938 ± 0.038 ± 0.149
4.525		1.612 ± 0.022 ± 0.076	0.457 ± 0.004 ± 0.029	1.941 ± 0.019 ± 0.143
4.575		1.602 ± 0.048 ± 0.076	0.456 ± 0.011 ± 0.029	1.940 ± 0.060 ± 0.144
4.625			0.456 ± 0.011 ± 0.037	1.927 ± 0.058 ± 0.157
4.675			0.447 ± 0.006 ± 0.030	1.898 ± 0.034 ± 0.145
4.725			0.443 ± 0.004 ± 0.031	1.881 ± 0.019 ± 0.146
4.775			0.441 ± 0.006 ± 0.035	1.839 ± 0.032 ± 0.150
4.825			0.442 ± 0.007 ± 0.035	1.847 ± 0.037 ± 0.152
4.875		1.556 ± 0.050 ± 0.071	0.433 ± 0.006 ± 0.029	1.811 ± 0.021 ± 0.144
4.925				1.793 ± 0.016 ± 0.162
4.975			0.430 ± 0.004 ± 0.027	1.795 ± 0.019 ± 0.138
5.025			0.430 ± 0.012 ± 0.026	1.795 ± 0.063 ± 0.137
5.075				1.781 ± 0.018 ± 0.151
5.125		1.499 ± 0.017 ± 0.032		1.756 ± 0.059 ± 0.146
5.175				1.753 ± 0.016 ± 0.125
5.225				1.774 ± 0.050 ± 0.154
5.275			0.418 ± 0.010 ± 0.027	1.737 ± 0.038 ± 0.136
5.325			0.419 ± 0.014 ± 0.024	1.739 ± 0.059 ± 0.133
5.375			0.416 ± 0.005 ± 0.024	1.710 ± 0.021 ± 0.125
5.425				1.706 ± 0.030 ± 0.149
5.475	1.545 ± 0.013 ± 0.032			1.704 ± 0.054 ± 0.154
5.525				1.647 ± 0.033 ± 0.144
5.625			0.404 ± 0.003 ± 0.020	1.643 ± 0.020 ± 0.113
5.925				1.603 ± 0.026 ± 0.098
5.955		1.436 ± 0.023 ± 0.027	0.374 ± 0.008 ± 0.011	1.472 ± 0.032 ± 0.052
6.915	1.521 ± 0.009 ± 0.014	1.404 ± 0.011 ± 0.027	0.361 ± 0.004 ± 0.010	1.389 ± 0.020 ± 0.044
7.267		1.376 ± 0.012 ± 0.036	0.353 ± 0.004 ± 0.012	1.363 ± 0.022 ± 0.065
7.630			0.343 ± 0.004 ± 0.019	1.308 ± 0.022 ± 0.125
8.021			0.336 ± 0.002 ± 0.012	1.274 ± 0.010 ± 0.052
8.847	1.508 ± 0.013 ± 0.015	1.325 ± 0.011 ± 0.027	0.329 ± 0.003 ± 0.010	1.215 ± 0.017 ± 0.044
9.775		1.281 ± 0.005 ± 0.038	0.313 ± 0.001 ± 0.010	1.146 ± 0.005 ± 0.041
10.267				1.156 ± 0.010 ± 0.031
10.762			0.306 ± 0.002 ± 0.007	1.115 ± 0.011 ± 0.029
11.344	1.500 ± 0.014 ± 0.010	1.242 ± 0.015 ± 0.021	0.299 ± 0.005 ± 0.008	1.084 ± 0.035 ± 0.033
12.580				1.049 ± 0.013 ± 0.022
13.238	1.503 ± 0.025 ± 0.023	1.205 ± 0.011 ± 0.019	0.287 ± 0.003 ± 0.006	1.001 ± 0.010 ± 0.026
14.689	1.520 ± 0.012 ± 0.011	1.216 ± 0.013 ± 0.027	0.285 ± 0.003 ± 0.010	0.992 ± 0.013 ± 0.048
17.108	1.478 ± 0.011 ± 0.017	1.112 ± 0.011 ± 0.038	0.256 ± 0.003 ± 0.011	0.900 ± 0.015 ± 0.039

Q^2 [(GeV/c)^2]	$M_2(Q^2)$x10^{-1}	$M_4(Q^2)$x10^{-2}	$M_6(Q^2)$x10^{-2}	$M_8(Q^2)$x10^{-3}
19.072		1.107 ± 0.010 ± 0.021	0.257 ± 0.003 ± 0.007	0.911 ± 0.014 ± 0.028
20.108	1.467 ± 0.010 ± 0.007	1.094 ± 0.014 ± 0.019	0.250 ± 0.004 ± 0.008	0.874 ± 0.016 ± 0.039
21.097	*1.486 ± 0.010 ± 0.011	1.101 ± 0.012 ± 0.032		
24.259	*1.470 ± 0.012 ± 0.014	1.052 ± 0.010 ± 0.040		
26.680	*1.469 ± 0.013 ± 0.007	1.056 ± 0.010 ± 0.021		
32.500	*1.479 ± 0.013 ± 0.014			
34.932	*1.445 ± 0.113 ± 0.007			
36.750	*1.482 ± 0.012 ± 0.018	1.014 ± 0.010 ± 0.016	0.223 ± 0.003 ± 0.004	0.767 ± 0.014 ± 0.014
43.970	*1.478 ± 0.026 ± 0.010			
47.440	*1.477 ± 0.127 ± 0.007	1.016 ± 0.029 ± 0.018		
64.270		9.450 ± 0.042 ± 0.014	0.206 ± 0.007 ± 0.003	0.699 ± 0.022 ± 0.010
75.000		*9.443 ± 0.017 ± 0.024	*0.206 ± 0.006 ± 0.008	
86.000		*9.183 ± 0.018 ± 0.019	*0.196 ± 0.007 ± 0.007	
97.690		*9.232 ± 0.019 ± 0.010	*0.199 ± 0.005 ± 0.003	*0.672 ± 0.023 ± 0.008

TABLE III: Extracted parameters of the twist expansion at the renormalization scale $\mu^2 = 10$ (GeV/c)^2. The first uncertainty is the systematic one described in text, while the second uncertainty has a statistical origin and is obtained from a MINOS [41] minimization procedure. The contribution of twists-6 to M_2 was too small to be extracted by the present procedure.

	M_2	M_4	M_6	M_8
$\eta_n(\mu^2)$	0.152±0.02±0.03	(1.215±0.03±0.01)×10^{-2}	(2.95±0.1±0.04)×10^{-3}	(1.05±0.02±0.02)×10^{-3}
$a^{(4)}$	(4±2±22)×10^{-4}	(7.4±2±2.5)×10^{-3}	(2.7±0.5±0.04)×10^{-3}	(1.7±0.8±0.04)×10^{-3}
$\gamma^{(4)}$	3.4±0.2±5.2	3±0.5±1	5.9±0.3±0.02	6.4±3.5±0.04
$a^{(6)}$	-	(-1.5±0.2±0.3)×10^{-2}	(-9.2±1.4±0.15)×10^{-3}	(-6.6±2±0.16)×10^{-3}
$\gamma^{(6)}$	-	1.9±0.4±0.8	4.3±0.3±0.02	4.7±1.4±0.04

applicable also at low Q^2. The corrections to the leading twist are significant but not crucial;

- the Q^2-behaviour of the data indicates the presence of the higher twist contribution at Q^2 <5 (GeV/c)^2, positive at large Q^2 and negative at Q^2 ∼1-2 (GeV/c)^2; the change of sign requires in Eq. 20 at least two higher twist terms with opposite signs. As already noted in Refs. [4, 23, 42], such a cancellation makes the total higher twist contribution smaller than its individual terms, which exceed the leading twist. This partial *cancellation is a manifestation of the duality phenomena in the pQCD representation* [45]. It leads to the prevailing DIS-inspired picture of virtual photon-nucleon collisions also at low Q^2. The same mutual cancellation of higher twist terms was observed in the proton structure function moments in Refs. [4, 46] and in the first neutron g_1 moment [47];

- the total higher twist contribution is significant at $Q^2 \approx$ few (GeV/c)^2 and large x. This can be seen by comparing the higher twist contribution to M_8, which is more heavily weighted in x, to M_2. For Q^2 >6 (GeV/c)^2 the higher twist contribution does not exceed ≃15% of the leading twist for all four moments.

Therefore, we have demonstrated that despite nuclear effects in the deuteron, a pQCD-based analysis of the deuteron structure function moments is sensible, so that a precise determination of the leading and higher twists is possible with the high quality of the new CLAS data. The extracted values of the reduced matrix elements O_{n2} still contain some contribution of the nuclear off-shell and Fermi motion effects, which should be taken care of before a comparison to Lattice QCD simulations is made. However, most of the nuclear effects, in particular FSI, should be absorbed in the effective higher twist terms due to their scale difference. An estimate of the leading twist nuclear corrections would allow extraction of the non-singlet part of the nucleon structure function moments, which can be directly tested in the Lattice QCD simulations.

Acknowledgments

This work was supported by the Istituto Nazionale di Fisica Nucleare, the French Commissariat à l'Energie Atomique, the French Centre National de la Recherche Scientifique, the U.S. Department of Energy and National Science Foundation and the Korea Science and Engineering Foundation. The Southeastern Universities Research Association (SURA) operates the Thomas Jefferson National Accelerator Facility for the United States Department of Energy under contract DE-AC05-84ER40150.

TABLE IV: The extracted leading twist contribution $\eta_n(Q^2)$ (see Eq. 17) shown in Fig. 12, reported with systematic uncertainties.

Q^2 [(GeV/c)^2]	$\eta_2(Q^2)$x10^{-1}	$\eta_4(Q^2)$x10^{-2}	$\eta_6(Q^2)$x10^{-3}	$\eta_8(Q^2)$x10^{-3}
1.025	1.84 ± 0.07	2.56 ± 0.06	11.5 ± 0.4	8.63 ± 0.07
1.075	1.83 ± 0.07	2.49 ± 0.05	10.6 ± 0.4	7.28 ± 0.06
1.125	1.82 ± 0.07	2.42 ± 0.05	9.88 ± 0.3	6.34 ± 0.05
1.175	1.81 ± 0.07	2.36 ± 0.05	9.29 ± 0.3	5.64 ± 0.05
1.225	1.80 ± 0.07	2.31 ± 0.05	8.80 ± 0.3	5.11 ± 0.04
1.275	1.79 ± 0.07	2.26 ± 0.05	8.38 ± 0.3	4.68 ± 0.04
1.325	1.78 ± 0.06	2.21 ± 0.05	8.02 ± 0.3	4.34 ± 0.04
1.375	1.77 ± 0.06	2.17 ± 0.05	7.70 ± 0.3	4.05 ± 0.03
1.425	1.77 ± 0.06	2.13 ± 0.05	7.43 ± 0.3	3.82 ± 0.03
1.475	1.76 ± 0.06	2.10 ± 0.05	7.18 ± 0.3	3.61 ± 0.03
1.525	1.75 ± 0.06	2.07 ± 0.05	6.96 ± 0.2	3.43 ± 0.03
1.575	1.74 ± 0.06	2.04 ± 0.04	6.76 ± 0.2	3.28 ± 0.03
1.625	1.74 ± 0.06	2.01 ± 0.04	6.58 ± 0.2	3.14 ± 0.03
1.675	1.73 ± 0.06	1.98 ± 0.04	6.41 ± 0.2	3.02 ± 0.02
1.725	1.72 ± 0.06	1.95 ± 0.04	6.26 ± 0.2	2.91 ± 0.02
1.775	1.72 ± 0.06	1.93 ± 0.04	6.12 ± 0.2	2.81 ± 0.02
1.825	1.71 ± 0.05	1.91 ± 0.04	6.00 ± 0.2	2.73 ± 0.02
1.875	1.70 ± 0.05	1.89 ± 0.04	5.88 ± 0.2	2.65 ± 0.02
1.925	1.70 ± 0.05	1.87 ± 0.04	5.76 ± 0.2	2.57 ± 0.02
1.975	1.69 ± 0.05	1.85 ± 0.04	5.66 ± 0.2	2.50 ± 0.02
2.025	1.69 ± 0.05	1.83 ± 0.04	5.56 ± 0.2	2.44 ± 0.02
2.075	1.68 ± 0.05	1.81 ± 0.04	5.47 ± 0.2	2.38 ± 0.02
2.125	1.68 ± 0.05	1.80 ± 0.04	5.39 ± 0.2	2.33 ± 0.02
2.175	1.67 ± 0.05	1.78 ± 0.04	5.31 ± 0.2	2.28 ± 0.02
2.225	1.67 ± 0.05	1.77 ± 0.04	5.23 ± 0.2	2.23 ± 0.02
2.275	1.66 ± 0.05	1.75 ± 0.04	5.16 ± 0.2	2.19 ± 0.02
2.325	1.66 ± 0.05	1.74 ± 0.04	5.11 ± 0.2	2.16 ± 0.02
2.375	1.66 ± 0.05	1.73 ± 0.04	5.05 ± 0.2	2.12 ± 0.02
2.425	1.66 ± 0.05	1.72 ± 0.04	5.00 ± 0.2	2.09 ± 0.02
2.475	1.65 ± 0.05	1.71 ± 0.04	4.94 ± 0.2	2.06 ± 0.02
2.525	1.65 ± 0.05	1.70 ± 0.04	4.89 ± 0.2	2.04 ± 0.02
2.575	1.65 ± 0.05	1.69 ± 0.04	4.85 ± 0.2	2.01 ± 0.02
2.625	1.64 ± 0.05	1.68 ± 0.04	4.80 ± 0.2	1.98 ± 0.02
2.675	1.64 ± 0.04	1.67 ± 0.04	4.76 ± 0.2	1.96 ± 0.02
2.725	1.64 ± 0.04	1.66 ± 0.04	4.71 ± 0.2	1.93 ± 0.02
2.775	1.64 ± 0.04	1.65 ± 0.04	4.67 ± 0.2	1.91 ± 0.02
2.825	1.64 ± 0.04	1.64 ± 0.04	4.64 ± 0.2	1.89 ± 0.02
2.875	1.63 ± 0.04	1.63 ± 0.04	4.60 ± 0.2	1.87 ± 0.02
2.925	1.63 ± 0.04	1.62 ± 0.04	4.56 ± 0.2	1.85 ± 0.02
2.975	1.63 ± 0.04	1.62 ± 0.04	4.53 ± 0.2	1.83 ± 0.01
3.025	1.63 ± 0.04	1.61 ± 0.04	4.49 ± 0.2	1.81 ± 0.01
3.075	1.63 ± 0.04	1.60 ± 0.04	4.46 ± 0.2	1.79 ± 0.01
3.125	1.62 ± 0.04	1.59 ± 0.04	4.43 ± 0.2	1.78 ± 0.01
3.175	1.62 ± 0.04	1.59 ± 0.03	4.40 ± 0.2	1.76 ± 0.01
3.225	1.62 ± 0.04	1.58 ± 0.03	4.36 ± 0.2	1.74 ± 0.01
3.275	1.62 ± 0.04	1.57 ± 0.03	4.34 ± 0.2	1.73 ± 0.01
3.325	1.62 ± 0.04	1.57 ± 0.03	4.31 ± 0.2	1.71 ± 0.01
3.375	1.61 ± 0.04	1.56 ± 0.03	4.28 ± 0.2	1.70 ± 0.01
3.425	1.61 ± 0.04	1.55 ± 0.03	4.25 ± 0.1	1.68 ± 0.01
3.475	1.61 ± 0.04	1.55 ± 0.03	4.23 ± 0.1	1.67 ± 0.01
3.525	1.61 ± 0.04	1.54 ± 0.03	4.20 ± 0.1	1.66 ± 0.01
3.575	1.61 ± 0.04	1.53 ± 0.03	4.18 ± 0.1	1.64 ± 0.01
3.625	1.61 ± 0.04	1.53 ± 0.03	4.15 ± 0.1	1.63 ± 0.01
3.675	1.61 ± 0.04	1.52 ± 0.03	4.13 ± 0.1	1.62 ± 0.01
3.725	1.60 ± 0.04	1.52 ± 0.03	4.11 ± 0.1	1.61 ± 0.01
3.775	1.60 ± 0.04	1.51 ± 0.03	4.08 ± 0.1	1.60 ± 0.01
3.825	1.60 ± 0.04	1.51 ± 0.03	4.06 ± 0.1	1.59 ± 0.01
3.875	1.60 ± 0.04	1.50 ± 0.03	4.04 ± 0.1	1.58 ± 0.01
3.925	1.60 ± 0.04	1.50 ± 0.03	4.02 ± 0.1	1.56 ± 0.01
3.975	1.60 ± 0.04	1.49 ± 0.03	4.00 ± 0.1	1.55 ± 0.01

Q^2 [(GeV/c)^2]	$\eta_2(Q^2)$x10^{-1}	$\eta_4(Q^2)$x10^{-2}	$\eta_6(Q^2)$x10^{-3}	$\eta_8(Q^2)$x10^{-3}
4.025	1.60 ± 0.03	1.49 ± 0.03	3.98 ± 0.1	1.54 ± 0.01
4.075	1.59 ± 0.03	1.48 ± 0.03	3.96 ± 0.1	1.53 ± 0.01
4.125	1.59 ± 0.03	1.48 ± 0.03	3.94 ± 0.1	1.52 ± 0.01
4.175	1.59 ± 0.03	1.47 ± 0.03	3.92 ± 0.1	1.52 ± 0.01
4.225	1.59 ± 0.03	1.47 ± 0.03	3.91 ± 0.1	1.51 ± 0.01
4.275	1.59 ± 0.03	1.46 ± 0.03	3.89 ± 0.1	1.50 ± 0.01
4.325	1.59 ± 0.03	1.46 ± 0.03	3.87 ± 0.1	1.49 ± 0.01
4.375	1.59 ± 0.03	1.46 ± 0.03	3.86 ± 0.1	1.48 ± 0.01
4.425	1.59 ± 0.03	1.45 ± 0.03	3.84 ± 0.1	1.47 ± 0.01
4.475	1.59 ± 0.03	1.45 ± 0.03	3.82 ± 0.1	1.46 ± 0.01
4.525	1.58 ± 0.03	1.44 ± 0.03	3.81 ± 0.1	1.46 ± 0.01
4.575	1.58 ± 0.03	1.44 ± 0.03	3.79 ± 0.1	1.45 ± 0.01
4.625	1.58 ± 0.03	1.44 ± 0.03	3.78 ± 0.1	1.44 ± 0.01
4.675	1.58 ± 0.03	1.43 ± 0.03	3.76 ± 0.1	1.43 ± 0.01
4.725	1.58 ± 0.03	1.43 ± 0.03	3.75 ± 0.1	1.43 ± 0.01
4.775	1.58 ± 0.03	1.43 ± 0.03	3.73 ± 0.1	1.42 ± 0.01
4.825	1.58 ± 0.03	1.42 ± 0.03	3.72 ± 0.1	1.41 ± 0.01
4.875	1.58 ± 0.03	1.42 ± 0.03	3.70 ± 0.1	1.40 ± 0.01
4.925	1.58 ± 0.03	1.41 ± 0.03	3.69 ± 0.1	1.40 ± 0.01
4.975	1.58 ± 0.03	1.41 ± 0.03	3.68 ± 0.1	1.39 ± 0.01
5.025	1.57 ± 0.03	1.41 ± 0.03	3.66 ± 0.1	1.38 ± 0.01
5.075	1.57 ± 0.03	1.40 ± 0.03	3.65 ± 0.1	1.38 ± 0.01
5.125	1.57 ± 0.03	1.40 ± 0.03	3.64 ± 0.1	1.37 ± 0.01
5.275	1.57 ± 0.03	1.39 ± 0.03	3.60 ± 0.1	1.35 ± 0.01
5.325	1.57 ± 0.03	1.39 ± 0.03	3.59 ± 0.1	1.35 ± 0.01
5.375	1.57 ± 0.03	1.39 ± 0.03	3.58 ± 0.1	1.34 ± 0.01
5.475	1.57 ± 0.03	1.38 ± 0.03	3.55 ± 0.1	1.33 ± 0.01
5.525	1.57 ± 0.03	1.38 ± 0.03	3.54 ± 0.1	1.33 ± 0.01
5.625	1.56 ± 0.03	1.37 ± 0.03	3.52 ± 0.1	1.32 ± 0.01
5.675	1.56 ± 0.03	1.37 ± 0.03	3.51 ± 0.1	1.31 ± 0.01
5.725	1.56 ± 0.03	1.37 ± 0.03	3.50 ± 0.1	1.31 ± 0.01
5.955	1.56 ± 0.03	1.35 ± 0.03	3.45 ± 0.1	1.28 ± 0.01
6.915	1.55 ± 0.03	1.31 ± 0.03	3.29 ± 0.1	1.21 ± 0.01
7.267	1.54 ± 0.02	1.30 ± 0.03	3.24 ± 0.1	1.18 ± 0.01
7.630	1.54 ± 0.02	1.28 ± 0.03	3.19 ± 0.1	1.16 ± 0.01
8.021	1.54 ± 0.02	1.27 ± 0.03	3.14 ± 0.1	1.14 ± 0.01
8.847	1.53 ± 0.02	1.24 ± 0.03	3.05 ± 0.1	1.10 ± 0.01
9.775	1.52 ± 0.02	1.22 ± 0.03	2.97 ± 0.1	1.06 ± 0.01
10.267	1.52 ± 0.02	1.21 ± 0.03	2.92 ± 0.1	1.04 ± 0.01
10.762	1.52 ± 0.02	1.20 ± 0.03	2.89 ± 0.1	1.02 ± 0.01
11.344	1.51 ± 0.02	1.19 ± 0.03	2.85 ± 0.1	1.00 ± 0.01
12.580	1.51 ± 0.02	1.16 ± 0.03	2.77 ± 0.1	0.97 ± 0.01
13.238	1.50 ± 0.02	1.15 ± 0.03	2.73 ± 0.1	0.95 ± 0.01
14.689	1.50 ± 0.02	1.13 ± 0.02	2.66 ± 0.09	0.92 ± 0.01
17.108	1.49 ± 0.01	1.10 ± 0.02	2.56 ± 0.09	0.88 ± 0.01
19.072	1.48 ± 0.01	1.08 ± 0.02	2.50 ± 0.09	0.85 ± 0.01
20.108	1.48 ± 0.01	1.07 ± 0.02	2.47 ± 0.09	0.84 ± 0.01
21.097	1.48 ± 0.01	1.06 ± 0.02	2.44 ± 0.09	0.83 ± 0.01
24.259	1.47 ± 0.01	1.04 ± 0.02	2.36 ± 0.08	0.80 ± 0.01
26.680	1.47 ± 0.01	1.03 ± 0.02	2.32 ± 0.08	0.78 ± 0.01
32.500	1.46 ± 0.01	1.00 ± 0.02	2.23 ± 0.08	0.74 ± 0.01
34.932	1.46 ± 0.01	0.99 ± 0.02	2.19 ± 0.08	0.73 ± 0.01
36.750	1.46 ± 0.01	0.98 ± 0.02	2.17 ± 0.08	0.72 ± 0.01
43.970	1.46 ± 0.01	0.96 ± 0.02	2.10 ± 0.07	0.69 ± 0.01
47.440	1.46 ± 0.01	0.95 ± 0.02	2.07 ± 0.07	0.68 ± 0.01
64.270	1.46 ± 0.01	0.91 ± 0.02	1.96 ± 0.07	0.63 ± 0.01
75.000	1.45 ± 0.01	0.89 ± 0.02	1.91 ± 0.07	0.61 ± 0.01
86.000	1.45 ± 0.01	0.88 ± 0.02	1.86 ± 0.07	0.60 ± 0.01
97.690	1.45 ± 0.01	0.86 ± 0.02	1.83 ± 0.06	0.58 ± 0.01

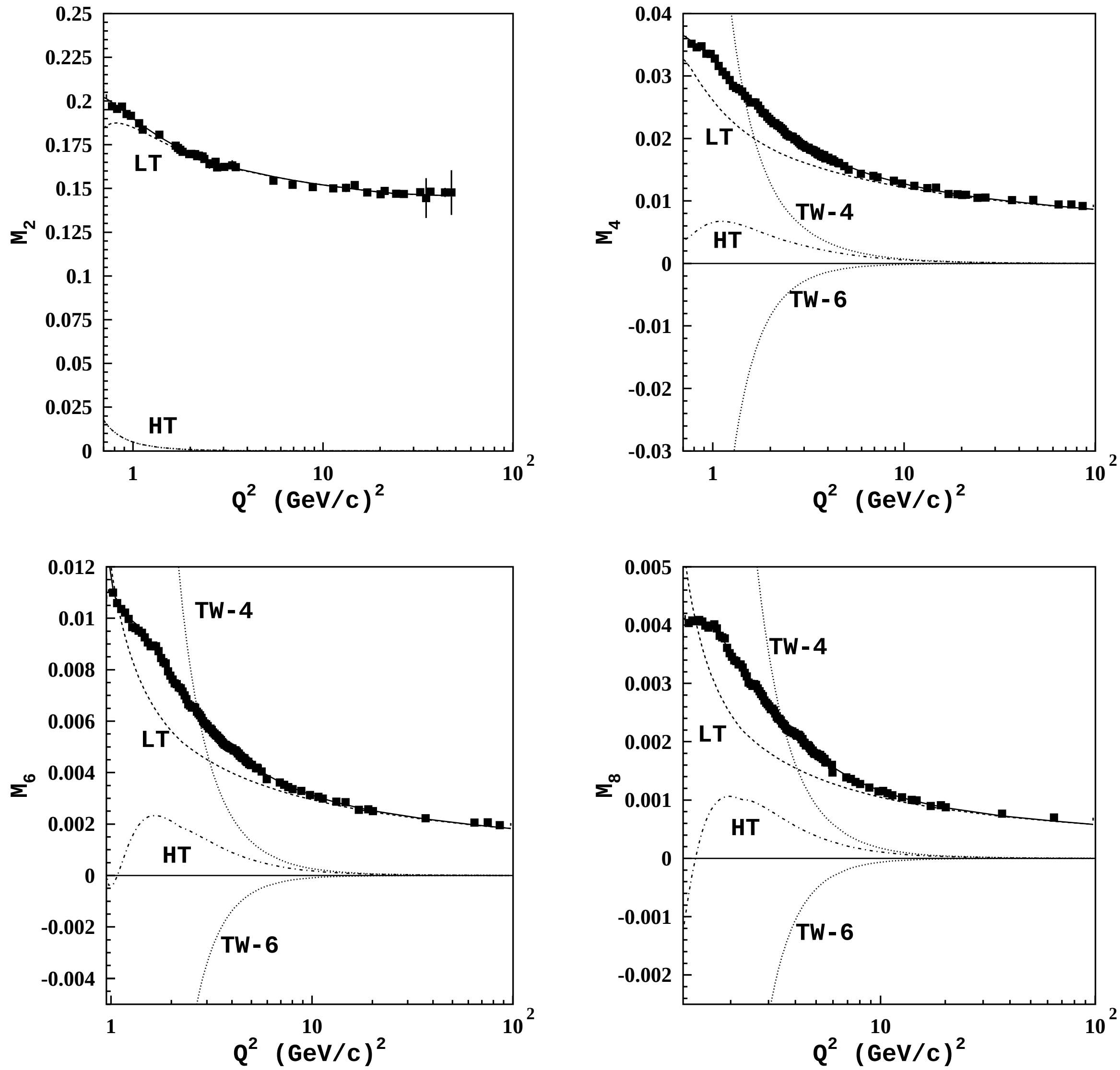

FIG. 12: Results of the twist analysis. The squares represent the Nachtman moments obtained in this analysis. The solid line is the fit to the moments using Eq. 16 with the parameters listed in Table III. The twist-2, twist-4, twist-6 and higher twist (HT) contributions to the fit are indicated. The twist-2 contribution was calculated using Eq. 17.

APPENDIX A: MODEL OF INCLUSIVE ELECTRON SCATTERING CROSS SECTION OFF THE DEUTERON AND THE DEUTERON STRUCTURE FUNCTION F_2

In order to extract efficiency, calculate radiative corrections and evaluate moments of the structure function F_2, it is essential to have a realistic model of the reaction cross section. Thanks to many previous experiments, comprehensive knowledge about electron-deuteron inclusive scattering is available. We based our model on these previous results. The model consists of three main elements:

- the elastic peak cross section was calculated using the deuteron elastic form-factors from Ref. [32, 48];
- the quasi-elastic peak cross section was obtained within a model of the nuclear structure of the deuteron [35] using elementary form-factors of the proton and neutron from Ref. [49]. This model is based on the De Forest [50] cc1 prescription for the off-shell nucleon and includes various sophisticated treatments of the final state interactions. Specifically designed for calculations of the quasi-elastic cross section for light and complex nuclei, it reproduces existing data very well (see Fig. 14);
- the inelastic cross section in the CLAS domain ($W^2 < 4.3$ GeV^2) was taken from the fit to the recent Hall C data [6];

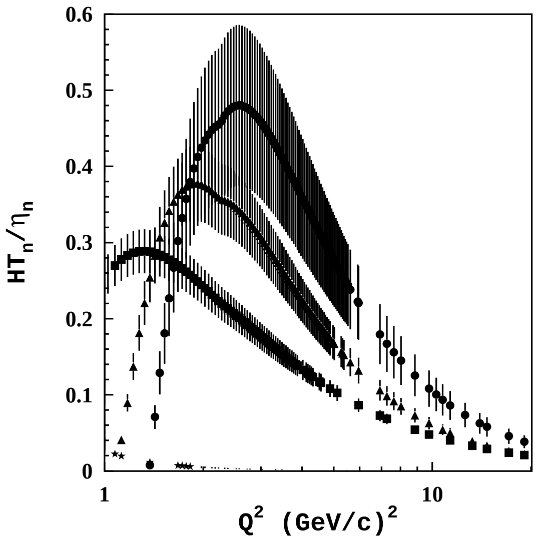

FIG. 13: Ratio of the total higher twist (see Eq. 20) to the leading twist given in Eq. 17 with its systematic uncertainties. Stars - M_2; squares - M_4; triangles - M_6; circles - M_8.

- in DIS we have chosen the parameterization from Ref. [51], which describes particularly well the low-x behaviour of the structure function.

The elastic peak is very small in our Q^2 range and hence it is only relevant for the radiative correction calculations. The inelastic cross section model, which fits the data from Hall C [6] very well, was obtained in the same kinematic domain. The quasi-elastic cross section calculations are model dependent and we have checked these before applying them to the data. Unfortunately, the Hall C data do not contain the quasi-elastic peak, therefore we had to compare to the previous SLAC and DESY measurements from Refs. [7, 15, 52]. Some of these data are not corrected for the radiative corrections, so we included radiative corrections in the model calculations. An example of the comparison of the quasi-elastic cross section model to the data, shown in Fig. 14, indicates an overall few percent agreement and a particularly good match on the low W^2 side of the peak, which is important for the determination of the higher moments.

At large Q^2 values, the parameterization from Ref. [51] fails to reproduce the data at high x. To correct the parameterization in this kinematic domain we switched to an older version of the fit reported in Ref. [53] for $x > 0.75$. However, in order to match the two fits we had to replace the x variable in the parameterization from Ref. [53] with $x' = x - 0.9(x - 0.75)^2$.

APPENDIX B: FIT OF THE RATIO $R \equiv \sigma_L/\sigma_T$

The ratio $R(x, Q^2)$ for the proton is well established in the DIS region and can be fairly well described by the SLAC fit from Ref. [54]. However, until recently experimental data in the resonance region were missing. The data from Hall C published in Ref. [55] cover the entire resonance region and extend down to very low Q^2 values. It was shown by the HERMES Collaboration in Ref. [56] that in DIS the ratio R does not depend on the nuclear mass number A. We take this assumption to be valid also in the resonance region. But since smearing effects of Fermi motion were expected to change both the F_2 and F_L structure functions, we performed a "smooth" parameterization of the measured ratio R. This smooth parameterization is based on the fit from Ref. [54], modified at low Q^2 values and large x by means of a multiplicative factor:

$$\Phi_Q = \left(\frac{Q^2}{Q_0^2}\right)^{C_Q} \exp\left[-B_Q C_Q \left(\frac{Q^2}{Q_0^2} - 1\right)\right] \quad \text{(B1)}$$
$$\left(1 - \frac{W_{th}^2 - C_W^2}{W^2}\right)^{B_W},$$

with $Q_0^2 = 0.8$ (GeV/c)^2, $C_Q = 0.729$, $B_Q = 2.14$, $C_W = 0.165$ GeV, $B_W = 0.383$ and where $W_{th} = M + m_\pi$ is the value of the invariant mass at the pion threshold.

In this way the resonance structures, clearly seen on the proton, were averaged out to a mean curve. The difference between these two models gave us an estimate of the systematic uncertainties of the ratio R, which turned out to be very small.

The ratio R under the quasi-elastic peak is a separate issue. Because of the nature of the quasi-elastic peak, R is no longer independent of A and should therefore be

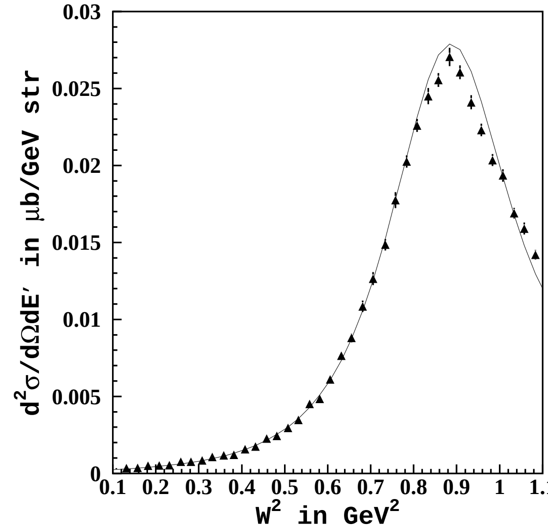

FIG. 14: Quasi-elastic cross section calculations in μb/(GeV str) from Ref. [35] compared to the experimental data from Ref. [7] at $E = 9.766$ GeV and $\theta = 10°$. The uncertainties are statistical only.

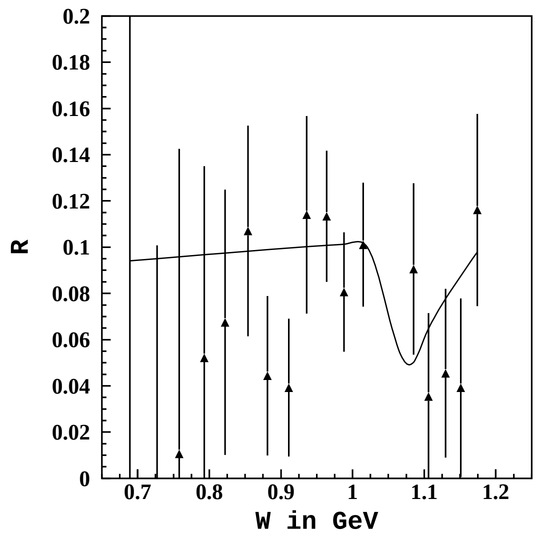

FIG. 15: Deuteron ratio $R = \sigma_L/\sigma_T$ in the quasi-elastic region as a function of W at $Q^2 = 3.25$ (GeV/c)^2. The points are from Ref. [57] and the curve represents the parameterization described in text. The minimum at $W = 1.07$ GeV is due to the pion electroproduction threshold.

treated within a nuclear model calculation. We used the model from Ref. [35], which treats separately the longitudinal and transverse nuclear response functions R_L and R_T to obtain the ratio R. The conventional ratio R can be calculated from those quantities as follows:

$$R = \frac{2Q^2}{Q^2+\nu^2}\frac{R_L}{R_T} \tag{B2}$$

The deuteron quasi-elastic ratio R obtained from this model was compared to the data on the ratio R for the deuteron [57] (see Fig. 15) and other nuclei [58] (deuteron data on R in the quasi-elastic region are scarce). Furthermore, the calculations were compared to the sum of the proton and neutron form factors, which simply implies:

$$R = \frac{G_E^2}{\tau G_M^2} \quad , \tag{B3}$$

where $\tau = Q^2/4M^2$ and G_E, G_M are sums of the known Sachs form-factors of the proton and neutron. Since the number of protons and neutrons is different in different nuclei we did not expect to have the same ratio R for all of them. At the same time the x-shape of the ratio is very similar from nucleus to nucleus. In the low Q^2 region, where precise data exist, the calculations reproduce the x-shape of the data reasonably well. The systematic uncertainty was estimated as a difference between the model calculation and the result of the naive form-factor sum given by Eq. B3.

[1] J.J. Aubert *et al.*, *Phys. Lett.* **B123**, 275 (1983).
[2] J.M. Cornwall and R.E. Norton, *Phys. Rev.* **177**, 2584 (1969).
[3] R.G. Roberts, *The structure of the proton*, Cambridge University Press (1990).
[4] M. Osipenko *et al.*, *Phys. Rev.* **D67**, 092001 (2003).
[5] G. Ricco *et al.*, *Phys. Rev.* **C57**, 356 (1998).
[6] I. Niculescu *et al.*, *Phys. Rev. Lett.* **85**, 1186 (2000); *Phys. Rev. Lett.* **85**, 1182 (2000).
[7] S. Rock *et al.*, *Phys. Rev.* **D46**, 24 (1992).
[8] S. Dasu *et al.*, *Phys. Rev.* **D49**, 5641 (1994).
[9] L.H. Tao *et al.*, *Z. Phys.* **C70**, 387 (1996).
[10] J.S. Poucher *et al.*, *Phys. Rev. Lett.* **32**, 118 (1974).
[11] A. Bodek, *Phys. Rev. Lett.* **51** 534 (1983); A. Bodek *et al.*, *Phys. Rev. Lett.* **50**, 1431 (1983); A. Bodek *et al.*, *Phys. Rev.* **D20**, 1471 (1979).
[12] S. Stein *et al.*, *Phys. Rev.* **D12**, 1884 (1975).
[13] W.B. Atwood *et al.*, SLAC-Report-185 (1975).
[14] M.D. Mestayer *et al.*, SLAC-Report-214 (1978).
[15] L.M. Stuart *et al.*, *Phys. Rev.* **D58**, 032003 (1998).
[16] A.C. Benvenuti *et al.*,*Phys. Lett.* **B237**, 592 (1989).
[17] M. Arneodo *et al.*, *Nucl. Phys.* **B483**, 3 (1997).
[18] M. Arneodo *et al.*, *Nucl. Phys.* **B487**, 3 (1997).
[19] M.R. Adams *et al.*, *Phys. Rev.* **D54**, 3006 (1996).
[20] M.R. Adams *et al.*, *Phys. Rev. Lett.* **75**, 1466 (1995).
[21] S. Catani *et al.*, CERN-TH/96-86; M. Cacciari and S. Catani, CERN-TH/2001-174.
[22] O. Nachtmann, *Nucl. Phys.* **B63**, 237 (1973).
[23] S. Simula, *Phys. Lett.* **B493**, 325 (2000).
[24] B. Mecking, *et al.*, *Nucl. Instr. and Meth.* **A503/3**, 513 (2003).
[25] M. D. Mestayer *et al.*, *Nucl. Instr. and Meth.* **A449**, 81 (2000).
[26] E. S. Smith *et al.*, *Nucl. Instr. and Meth.* **A432**, 265 (1999).
[27] G. Adams *et al.*, *Nucl. Instr. and Meth.* **A465**, 414 (2001).
[28] M. Amarian *et al.*, *Nucl. Instr. and Meth.* **A460**, 460 (2001).
[29] M. Osipenko *et al.*, CLAS-Note-03-001 (2003); hep-ex/0309052.
[30] M. Osipenko *et al.*, CLAS-Note-04-020 (2004).
[31] P. Bosted, CLAS-Note-04-004 (2004).
[32] K. Abe *et al.*, *Phys. Rev.* **D58**, 112003 (1998).
[33] L.W. Mo and Y.S. Tsai, *Rev. Mod. Phys.* **41**, 205 (1969); Yung-Su and Tsai, *Phys. Rev.* **122**, 1898 (1961).
[34] I. Sick, *Nucl. Phys.* **A218**, 509 (1974); A. Honegger-Feigenwinter, PhD thesis, University of Basel (1999).
[35] C. Ciofi degli Atti and S. Simula, *Phys. Rev.* **C53**, 1689 (1996).
[36] http://improv.unh.edu/Maurik/gsim_info.shtml.
[37] M. Osipenko *et al.*, CLAS-Note-05-001 (2005); hep-ex/0309052.
[38] I. Akushevich *et al.*, *Acta Phys. Polon.* **B28**, 563 (1997).

[39] D. Allasia *et al.*, *Z. Phys.* **C28**, 321 (1985).
[40] V. Barone, C. Pascaud and F. Zomer *Eur. Phys. J.* **C12**, 243 (2000).
[41] http://wwwinfo.cern.ch/asd/cernlib/overview.html.
[42] G. Ricco *et al.*, *Nucl. Phys.* **B555**, 306 (1999).
[43] Particle Data Group, D.E. Groom *et al.*, *Eur. Phys. Jour.* **C15**, 1 (2000).
[44] X. Ji and P. Unrau, *Phys. Rev.* **D52**, 72 (1995); U.K. Yang and A. Bodek, *Phys. Rev. Lett.* **82**, 2467 (1999).
[45] E. Bloom and F. Gilman, *Phys. Rev. Lett.* **25**, 1140 (1970); *Phys. Rev.* **D4**, 2901 (1971).
[46] M. Osipenko *et al.*, *Phys. Rev.* **D71**, 054007 (2005).
[47] Z.E. Meziani *et al.*, *Phys. Lett.* **B613**, 148 (2005). A. Deur *et al.*, *Phys. Rev. Lett.* **93**, 212001 (2004).
[48] C.D. Buchanan and M.R. Yearian, *Phys. Rev. Lett.* **15**, 303 (1965); J. E. Elias *et al.*, *Phys. Rev.* **177**, 2075 (1969); S. Galster *et al.*, *Nucl. Phys.* **B32**, 221(1971); R. G. Arnold *et al.*, *Phys. Rev. Lett.* **35**, 776 (1975); S. Auffret *et al.*, *Phys. Rev. Lett.* **54**, 649 (1985); R. Cramer *et al.*, *Z. Phys.* **C29**, 513 (1985); P. Bosted *et al.*, *Phys. Rev.* **C42**, 38 (1990).
[49] P.E. Bosted *et al.*, *Phys. Rev.* **C51**, 409 (1995).
[50] T. De Forest and J.D. Walecka, *Adv. Phys.* **15**, 1 (1966).
[51] B. Adeva *et al.*, *Phys. Rev.* **D58**, 112001 (1998).
[52] W. Albrecht *et al.*, *Phys. Lett.* **26B**, 642 (1968).
[53] P. Amaudruz *et al.*, *Nucl. Phys.* **B371**, 3 (1992).
[54] K. Abe *et al.*, *Phys. Lett.* **B452**, 194 (1999).
[55] Y. Liang *et al.*, nucl-ex/0410027, Jefferson Lab experiment E94-110.
[56] K. Ackerstaff *et al.*, *Phys. Lett.* **B475**, 386 (2000); Erratum-ibid. **B567**, 339 (2003).
[57] A. Lung *et al.*, *Phys. Rev. Lett.* **70**, 718 (1993).
[58] P. Barreau *et al.*, *Nucl. Phys.* **A402**, 515 (1983); A. Zighiche *et al.*, *Nucl. Phys.* **A572**, 513 (1994); A. Hotta *et al.*, *Phys. Rev.* **C30**, 87 (1984); T.C. Yates *et al.*, *Phys. Lett.* **B312**, 382 (1993); C. Marchand *et al.*, *Phys. Lett.* **B153**, 29 (1985); Z.E. Meziani *et al.*, *Phys. Rev. Lett.* **52**, 2130 (1984); Z.E. Meziani *et al.*, *Phys. Rev. Lett.* **54**, 1233 (1985); S.A. Dytman *et al.*, *Phys. Rev.* **C38**, 800 (1988); K. Dow *et al.*, *Phys. Rev. Lett.* **61**, 1706 (1988); C.C. Blatchley *et al.*, *Phys. Rev.* **C34**, 1243 (1986); R. Altemus *et al.*, *Phys. Rev. Lett.* **44**, 965 (1980); M. Deady *et al.*, *Phys. Rev.* **C28**, 631 (1983).